Injury Mechanism and Threshold of Acute First Metatarsophalangeal Joint Sprains

---

A Thesis

Presented to

the faculty of the School of Engineering and Applied Science

University of Virginia

---

in partial fulfillment

of the requirements for the degree

Master of Science

by

Rebecca Elizabeth Frimenko

May

2013

APPROVAL SHEET

The thesis

is submitted in partial fulfillment of the requirements

for the degree of

Master of Science

Rebecca Frimenko

AUTHOR

The thesis has been read and approved by the examining committee:

Dr. Richard Kent

Advisor

Dr. Jeff Crandall

Dr. Silvia Blemker

Accepted for the School of Engineering and Applied Science:

James H. Ay

Dean, School of Engineering and Applied Science

May

2013

Abstract

Turf toe, or sprain of the first metatarsophalangeal (1MTP) joint, is a devastating injury to football players and accounts for a large amount of lost playing time. It is estimated that 45% of professional players sustain 1MTP sprain throughout their career (Rodeo et al. 1993). Despite the prevalence and severity of the injury, current research has neither examined the mechanisms of injury nor described the tolerance of the joint. The goal of this thesis is to identify an injury mechanism and to quantify the tolerance of 1MTP joint to sprain in an *in vitro* cadaveric model.

To this end, cadaveric limbs were tested to varying degrees of hyperextension while recording kinematic and kinetic parameters. Specimens were examined for injury post-test by medical professionals. Binary logistic regression was performed to assess the discriminating properties of recorded parameters, and a survival analysis was performed on the most useful parameters to assess risk of injury. Injury risk was compared to previously obtained athlete performance data to evaluate performance-injury risk tradeoff.

Twenty lower limbs (right and left) were tested. Injury was identified in 11 of these specimens. Both maximum hyperextension angle and maximum moment through the 1MTP joint were found to predict injury ($\gamma_{\text{max. angle, hallux,}}$=0.61, $\gamma_{\text{max. moment}}$ =0.61). Because it is non-dimensional, hyperextension angle was identified as the most valuable discriminating parameter. The 50% risk of 1MTP sprain was found to occur at 86° of extension.

Athletic performance data collected from professional football players were used to develop a cumulative probability function for the maximum 1MTP joint angle found during several tasks. This function was found to be offset from the injury risk function. For example, 50% of peak extension angles attained during running are below 52°, which is 34° less than the angle corresponding to 50% risk of injury. This offset between the performance distribution and the injury risk function is considered to be a design space within which athletic shoes may be designed to reduce injury risk without compromising athletic performance.

Acknowledgements

This thesis is for my parents. The confidence and courage necessary to attempt, and the support and encouragement to fuel completion, all come from them.

Acknowledgment and gratitude are due to my committee: Dr. Richard Kent, advisor; Dr. Jeff Crandall, committee chair; Dr. Silvia Blemker, mentor. I would like to thank the NFL and the members of the Foot & Ankle Subcommittee of the NFL for funding, supporting and providing valuable input to this study. This study was performed at the University of Virginia Center for Applied Biomechanics and sponsored by Biomechanics Consulting and Research (BioCore), LLC.

Chapter List

List of Figures

List of Tables

List of Symbols

0°	1MTP zero-angle alignment
1MTP	first metatarsophalangeal (joint)
6DoF	six degree-of-freedom (motion)
d	instantaneous vector from 1MTP joint center to the hallux center of pressure
F	force applied to the hallux
F_{ROI}	load through the region of interest around the hallux as determined by the pressure mat
F_{Total}	load through the entire pressure mat
f(x)	probability density function
F(x)	cumulative density function
H(x)	hazard function
M	calculated moment at the 1MTP joint during testing
M1	first metatarsal
N_c	number of concordant pairs
N_d	number of discordant pairs
P^I	percent risk of injury
PP1	proximal phalanx of the first ray
S(x)	survival function
T	motion capture transformation matrix
x	tested stimulus value
X	stimulus value at injury

$\boldsymbol{\beta}$ transformation matrix between hallux motion-capture coordinate system and M1 coordinate system

γ Goodman-Kruskal's Gamma

$\Delta\theta_{hallux}^{\max}$ maximum change in 1MTP extension angle from start of test

θ_{tp} maximum toe plate rotation angle

$\theta_{hallux}^{t=0}$ 1MTP angle at the start of test

$\theta_{hallux}^{\max}$ maximum 1MTP extension angle

θ_{BB} bone-based extension angle

θ_{SB} skin-based extension angle

$\boldsymbol{\lambda}$ transformation matrix from pressure mat coordinate system to motion-capture coordinate system

$\boldsymbol{\eta}$ matrix of hallux motion capture markers in the hallux coordinate system

1. Introduction

1.1. Motivation

Sprain to the 1st metatarsophalangeal (1MTP) joint, colloquially termed turf toe (Bowers and Martin 1976), is a potentially debilitating injury to elite athletes because the hallux, great toe, plays a pivotal role in an athlete's ability to run and cut. The hallux supports more than twice the load of the other toes during athletic activities such as running, jumping, and cutting (Stoke et al, 1979, Hetherington et al. 1992, Ford et al. 2006, Orendurff et al. 2008). Thus, injury to the 1MTP joint in athletes results in a large amount of playing time lost. Coker et al. (1978) reported that injuries to the 1MTP joint caused more time lost for collegiate American football players than ankle injuries, despite the fact that ankle injuries occurred over four times more frequently. Clanton et al. (1986) found that 1MTP sprains have an average time-loss of 6 days, with a range of 0 to 56 days. These injuries are also common. Kaplan et al. (2011) found 1MTP sprains to be the third most common foot/ankle injury of collegiate players at the NFL Scouting combine, and Rodeo et al. (1993) estimated that 45% of professional football players will sustain a 1MTP sprain during their career.

Though this athletic injury is most commonly associated with American football, it occurs in other sports as well. Numerous case studies and reports of these injuries refer to sports such as basketball (Coker et al. 1978, Mullis and Miller 1980, Badekas et al. 2009), gymnastics (Wilson et al. 2005, Badekas et al. 2009), running (Kubitz 2003), and soccer (Fabeck et al. 2002, Manning and Levy 2006, Badekas et al. 2009).

It may be possible to design shoes or orthotics to reduce the risk of 1MTP sprain, but there have been no studies which quantify injury risk in relation to functional anatomy. Previous research has focused on retrospective, epidemiological analyses and case studies of professional, elite athletes (Rodeo et al. 1993, Meyer et al. 1994). From these studies, situational factors which may increase risk of injury have been suggested: type of playing surface (Bowers and Martin 1974, Rodeo et al. 1993), player position (Rodeo et al.1993, Eggert 1990), and shoe type (Bowers and Martin 1974). Other studies have focused on anatomical conditions which may predispose an athlete to injury (Eggert 1990, Brophy et al. 2009, Rodeo et al. 1993). However, these studies have not linked measurable engineering parameters to injury risk. Prieskorn et al. (1995) attempted to generate 1MTP sprain in a cadaver model, but the reported injuries and number of tested specimens is insufficient for the development of an injury risk function. Therefore, the goals of this thesis are to create clinically-relevant 1MTP sprain in cadaver specimens, to identify measureable parameters that predict injury, to formulate injury risk functions that relate measureable parameters to injury risk, and to interpret these injury risk functions relative to the foot kinematics required for athletic performance.

The following sections describe the salient anatomic components of the 1MTP joint and the functional anatomy relating to injury mechanisms.

1.2. Anatomy

1.2.1. Bones

The 1MTP joint is composed of four bones: the first metatarsal (M1), the proximal phalanx of the first ray (PP1), and two sesamoids – medial and lateral (*Figure 1*).

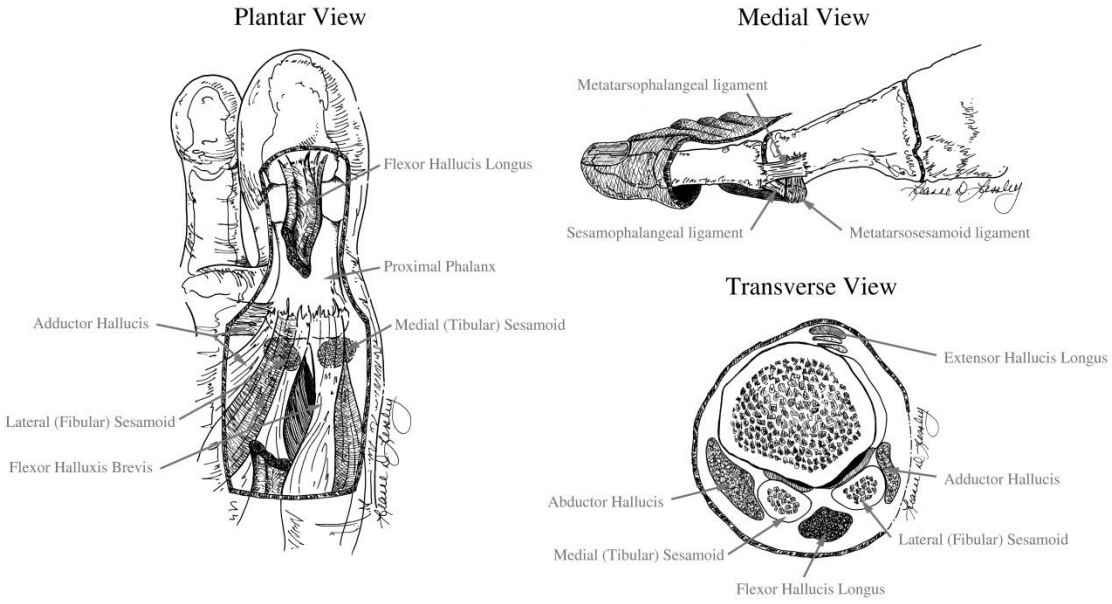

Figure 1 - bones and muscles of the first metatarsophalangeal (1MTP) joint. Reprinted from Frimenko et al. (2012) with permission from Begell House, Inc.

The head of M1 has a shallow, convex shape which articulates with the base of the proximal phalanx. These two bones act as a hinge joint, with primary rotation occurring as dorsiflexion and plantarflexion. Descriptions of the range of motion vary based upon the definition of zero-angle, but all sources agree that there is more dorsiflexion motion than plantarflexion (*Table 1*). Out-of-plane motion is limited to approximately 15° ad/abduction (Nevin 1997).

Table 1 – passive range of motion of the 1MTP joint

Study	Dorsiflexion (deg)	Total range of motion (deg)
Joseph 1954	73	-
Shereff et al. 1986	76	111
Buell et al. 1988	82	97
Eggert 1990	72	109
Nawoczenski et al. 1999	57	94

The sesamoid bones are ossified sections of muscle tendon which typically form between the ages of nine and 11 years (McCormick and Anderson 2009). Because of myriad centers of ossification, sesamoids occurring in two pieces (bipartite) or three pieces (tipartite) are not uncommon (Rodeo et al. 1993). Bipartite or tripartite sesamoids may also result from fracture due to trauma. The medial and lateral sesamoids bones are roughly equal in size, convex on the plantar aspect, and concave on the dorsal aspect (Karadaglis and Grace 2003). During 1MTP extension and flexion, the sesamoids ride over the M1 head in individual grooves. Richardson (1987) proposed three functions of the sesamoids: provide a mechanical advantaged to muscles and tendons, serve as shock absorbers, and protect the flexor halucix longus (FHL).

1.2.2. Muscles

Though this thesis will not analyze the effects of active muscles on injury, the presence of muscles plays an important role in defining joint kinematics. For example, the sesamoids are ossified sections of the distal flexor hallucis brevis (FHB) tendon. The FHB originates on the plantar surfaces of the cuboid and lateral cuneiforms. The muscle belly is divided into two sections (medial and lateral), but these sections merge to insert together on the base of the proximal phalanx of the hallux.

Along with the FHB, the tendons of the abductor hallucis (ABH) and adductor hallucis (ADH) contribute to the ligamentous plantar plate structure. The ABH originates on the medial process of the calcaneal tuberosity and inserts with the FHB on the proximal-medial head of the proximal phalanx of the hallux (Seireg and Arvikar 1989). The ADH consists of two distinct muscle bellies: the oblique portion which originates on the bases of the second, third, and fourth metatarsals, and the oblique portion which originates on the heads of the third, fourth, and fifth metatarsals. Both the oblique and transverse ADH insert on the lateral side of the base of the proximal phalanx. These three intrinsic, planar muscles act to flex the hallux and control 1MTP ad/abduction.

The flexor hallucis longus (FHL) is a 1MTP flexor extrinsic to the foot. The FHL originates on the lower two-thirds of the posterior surface of the fibula (Seireg and Arvikar 1989). The FHL tendon descends to the plantar side of the foot through the tarsal tunnel and passes between, and plantar to, the sesamoids before inserting on the distal phalanx of the hallux.

Two muscles serve to help extend the big toe: extensor hallucis longus (EHL) and extensor hallucis brevis (EHB). The EHL originates on the lateral, anterior side of the fibula and inserts on the base of the distal phalanx of the hallux. The EHB originates on the calcaneus and crosses to the dorsum of the foot before inserting on the first proximal phalanx.

Though it does not act directly on the 1MTP joint, the triceps surae is functionally important to the development of 1MTP sprain. The three muscles making up the triceps surae (medial and lateral gastrocnemius and the soleus), insert on the calcaneus through

the Achilles's tendon. In children and young adults, this tendon wraps around the calcaneus to the plantar side of the foot to become the plantar aponeurosis (Snow et al. 1995). With age, the continuity of these fibers diminishes until the two are effectively separate structures. Beyond contributing to the plantar aponeurosis, the triceps surae is important as the main plantar flexors of the foot.

1.2.3. Ligaments

During 1MTP sprain, the injured structure is a ligamentous cloud surrounding the 1MTP joint called the plantar plate (Coker et al. 1978, Tewes et al. 1994, Fabeck et al. 2002, McCormick and Anderson 2009). The plantar plate connects the M1, PP1, and the two sesamoids. This structure can be subdivided into four ligaments: intersesamoid, sesamophalangeal, and medial and lateral metatarsosesamoid ligaments. The intersesamoid ligament is a transverse band which connects the medial and lateral sesamoids. The sesamophalgeal ligament runs from each of the sesamoids to the insertion on the proximal phalanx. The medial and lateral metatarsosesamoid ligaments connect the sesamoids to the medial or lateral aspect of the M1 head, respectively. Though these and other naming conventions are used throughout literature, it should be emphasized that the plantar plate is a continuous set of ligamentous fibers (Sarrafian 1993, Frimenko et al. 2012). The names of individual ligaments are a convenience of anatomical textbooks and academic literature only, without any discontinuity between the named structures.

The plantar plate generally refers to the ligaments parallel and distal to the sesamoids. The structures immediately proximal to the plantar plate include the tendons

of the FHB, the ABH, the ADH, and the plantar aponeurosis. The plantar aponeurosis, synonymously called the plantar fascia, is a longitudinally arranged bundle of dense fibrous connective tissue running from the calcaneus to the proximal phalanx of each digit (Hicks 1954). During childhood, this structure is continuous with the Achilles's tendon; with aging, these two become discrete (Snow et al. 1995).

1.3. Functional Anatomy and Injury Mechanisms

1.3.1. Hick's Windlass Mechanism

Hick's windlass mechanism is used to describe how the longitudinal arch of the foot is raised during 1MTP extension. The plantar aponeurosis together with the plantar plate wraps around the head of M1, which represents a pulley or winch. Because the plantar aponeurosis is anchored to the calcaneus, the calcaneus is drawn closer to the head of M1 when the hallux is extended, and as a result the longitudinal arch of the foot is raised (*Figure 2*). The mechanical windlass system of rope and winch helps to visualize how the position of the longitudinal arch of the foot, the calcaneus, the plantar aponeurosis, and hallux extension are related.

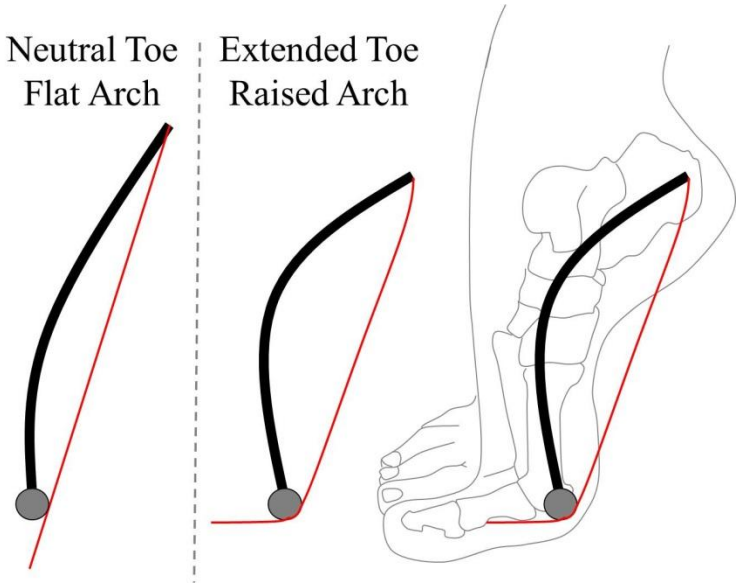

Figure 2 - Hick's Windlass mechanism. The thick line represents the longitudinal arch of the foot. The thin line represents the tendinous link of the plantar aponeurosis and plantar plate running from the calcaneus to the first proximal phalanx.

In the same way, this mechanism explains the relationship between ankle position and 1MTP range of motion. The sagittal plane rotation of the calcaneus, and, therefore, the origin of the plantar aponeurosis, is determined by ankle position (dorsiflexion, neutral, or plantarflexion). As the foot is rotated during ankle dorsiflexion, the relative position of the calcaneus lowers the longitudinal arch of the foot. Because of this, the origin of the plantar aponeurosis is moved away from the M1 head. As a result of the initial displacement, the plantar aponeurosis resists sesamoids motion earlier in hallux extension. The restricted sesamoid motion resists 1MTP extension through the plantar plate. Thus, the 1MTP joint has a smaller ROM when the ankle is dorsiflexed compared to when the ankle is plantarflexed.

1.3.2. Injury Mechanisms

The term "turf toe" was initially defined as a "sprain of the plantar capsule-ligament of the great toe metatarsophalangeal joint" (Bowers and Martin 1976). Since the coining of the term "turf toe," three mechanisms of 1MTP sprain have been generally accepted throughout literature: hyperextension (hyper-dorsiflexion), hyperflexion (hyper-plantarflexion), and valgus/varus loading of the hallux relative to the first metatarsal (*Figure 3*) (Eggert 1990).

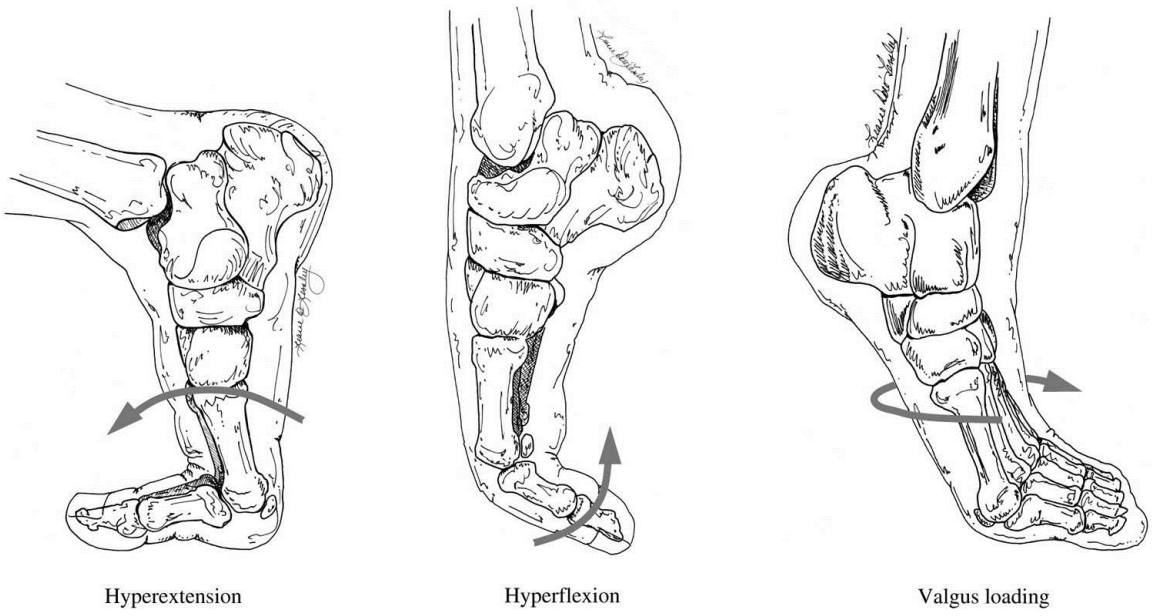

Figure 3 - suggested injury mechanisms for 1MTP sprain. Reprinted from Frimenko et al. (2012) with permission from Begell House, Inc.

1MTP sprain commonly occurs when an external force, such as that produced by a tackling player, is applied to the leg of a player whose forefoot is fixed on the ground. The delivery of axial load to a foot fixed in equinus drives the player's 1MTP joint into hyperextension (Bowers and Martin 1976). In a retrospective survey involving 80 active, professional football players and their trainers, Rodeo et al. (1993) found that, among the

45% of players who had sustained a turf toe injury, 85% of them had reported hyperextension to the 1MTP joint as the injury mechanism. The reported mechanism of hyperextension is consistent with an earlier survey of 66 collegiate athletic trainers, in which hyperextension was identified as the most common mechanism of 1MTP injury (Coker et al. 1978).

In a survey of football players and their trainers conducted by Rodeo et al. (1993), hyperflexion was the second most common injury mechanism (12%) and valgus or varus forces were the least common (4%). Because of the overwhelming implication of hyperextension in football 1MTP sprains, this injury mechanism is targeted in this thesis.

1.3.3. Acuteness and Chronicity

The previous section, and the majority of literature, treats 1MTP sprains as resulting from acute trauma (e.g Allen et al. 2004, McCormick and Anderson 2009). However, some case studies and reports suggest a chronic aspect to 1MTP sprain arising from repeated motion to the ROM limit (e.g. Manning and Levy 2006). The work herein focuses on acute injury.

1.4. Focus and Significance

The purpose of this research is to generate clinically-relevant 1MTP sprains through an *in vitro* cadaver model and to develop injury risk functions relating measurable parameters to the risk of this injury. Though it is out of the scope of this thesis to transform the cadaver-based injury risk function to a risk assessment based upon

living, elite athletes, the final chapter of this work will compare the cadaver-based injury risk function to elite athlete performance demands.

Means of increasing the safety of a sport include rule changes to enforce safe play and the use of safety equipment such as padding and helmets. The effectiveness of these injury reduction strategies increases with enhanced knowledge of the mechanics and thresholds of injury. The research conducted for this thesis will provide an understanding of injury mechanisms which may eventually be used as a basis for designing protective equipment. Similarly, the structural tolerances of these joints, described through this research, may be used to design the limits of safety equipment.

2. *In Vitro* Injury Creation

2.1. Background

The use of post-mortem human subjects (PMHS), cadavers, is integral to the investigation of injury biomechanics. Anthropomorphic Test Devices (ATD), colloquially known as test dummies, and finite element (FE) models can be useful; however, these tools are only accurate if relevant anatomy is represented and model components are validated by testing. Contemporary ATDs have been designed with a solid foot section, without any metatarsophalangeal joints. Clearly these devices are not suitable for testing 1MTP sprain. And while FE models may contain all the necessary anatomical structures, constitutive models for the plantar plate have never been developed, and models have never been tested in 1MTP extension. For these reasons, it is necessary to use PMHS tests to accurately describe 1MTP sprain. These tests will describe quantifiable parameters to interpret how and when injury occurs.

The over-arching goal of testing is to quantify meaningful variables in a way that is useful to predict injury and, ultimately, to define parameters for shoe or safety equipment design. Specifically, testing will help accomplish these larger goals by producing both sub-injurious and clinically-relevant injurious trials through an accepted injury mechanism while recording kinematic and kinetic parameters.

2.1.1. Motion Capture Methods

Visual motion analysis has played an important role in the modern study of biomechanics. One system for this type of analysis utilizes light reflected off of markers,

captured by cameras at several different viewpoints, and analyzed with specialized software (e.g. Vicon Nexus) to precisely identify markers in a predetermined coordinate system with respect to both global landmarks and to each other. Rigid body dynamics may be determined from pre-placing markers on the skin over significant anatomical landmarks and coordinating the measured motion with force components measured by plates embedded in the floor. Models such as OpenSim (http://opensim.standford.edu) can be modified with anthropometry taken from individual subjects and used in conjunction with motion capture analysis to describe participant-specific kinematics and kinetics.

Though initially developed for use in gait analysis, motion capture techniques have been adapted for use in impact testing of cadavers (e.g., Shaw et al. 2009). An array of high speed motion-capture cameras and sets of motion capture markers rigidly attached to bone directly depict motion of the bone rather than the overlying soft tissue. The high speed cameras allow dynamic events to be recorded and analyzed at sampling rates of up to 1,000 Hz.

2.1.2. Performance Evaluation

A dynamic performance evaluation of professional football players was conducted at the Indiana University Motion Analysis Research Laboratory (MARL) (Riley et al. 2012). This performance study was conducted to assess the natural ROM of elite athletes that occur during athletic events. This study provided the baseline inputs from which the PMHS test fixture was designed, and is summarized in the following paragraphs.

Methods

At MARL, nine professional football players performed three tasks, modified to fit within the confines of the gait lab: 3-cone drill, shuttle run, and vertical jump. In order to account for the range of skill sets and anthropometry seen in a professional football team, players were drawn in equal numbers from three player classes: power players (linemen), speed players (running backs and receivers), and hybrid players (linebacker and tight ends). Each athlete participated in bare feet and was outfitted with the Vicon (Centennial, CO, USA) Plug-In-Gait whole-body motion-capture marker set, modified to include additional foot markers (*Figure 4*). Markers were placed on the heel (calcaneus), the bases of the first and fourth metatarsals, the heads of the first and fourth metatarsals, and the hallux. Seven Vicon cameras recording at 240 Hz and two force plates (AMTI, Watertown, MA, USA) were used to record motion and ground reaction forces.

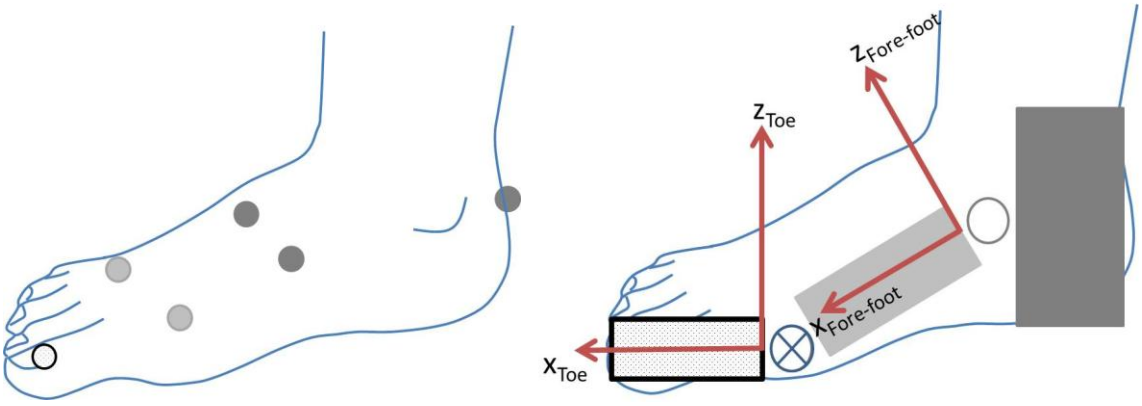

Figure 4 - motion capture marker set used for athlete performance analysis and model with coordinate system used to calculate 1MTP extension.

In post-test processing, the position of each marker was determined using Vicon Nexus software. This kinematic information was correlated with the force plate data in modified OpenSim musculoskeletal models, based on the anthropometry of each player. A model was created and analyzed for each player consisting of a hind-foot segment (calcaneus and tarsal bones), a fore-foot segment (metatarsals), and a toe segment (phalanges) (Figure 4). A ball joint, defined common to both the hind-foot and fore-foot segments, provided a rotation-only link between these two segments. A mediolateral revolute joint was imposed at the 1MTP joint to describe 1MTP extension. Sagittal plane motion, 1MTP extension, was described about this joint. Two coordinate systems were imposed to determine extension angle. On the fore-foot segment, the x-axis ran from joint connecting the hind-foot and fore-foot segment to the center of the distal end of the fore-foot segment. The y-axis was mediolateral, and the z-axis was orthogonal. On the toe segment, the x-axis ran from center of the segment base to the center of the segment head. The y-axis was mediolateral, and the z-axis was orthogonal. 1MTP extension angle was calculated as the angle between the x-axis of the fore-foot segment and x-axis of the toe segment. Stance phase was determined by correlating this kinematic description of motion with the force plate data.

Results

Of the nine tested players, one player (Speed Player 1) did not retain enough visible markers during testing to be used in analysis. The 1MTP maximum extensions for eight players are shown in *Table 2*:

Table 2 - 1MTP maximum extension (deg.) for eight athletes.

Task	Hybrid Players			Power Players			Speed Players		Average	Standard Deviation
	HP1	**HP2**	**HP3**	**PP1**	**PP2**	**PP3**	**SP2**	**SP3**		
Walk	85.8	73.7	74.0	80.8	74.6	58.2	67.1	78.1	**74.0**	**8.5**
Run	73.4	89.5	79.9	82.7	78.2	71.1	78.1	86.7	**79.9**	**6.2**
Cut	69.1	73.5	81.4	67.0	66.1	54.5	80.3	67.3	**69.9**	**8.6**
Start	73.5	74.1	97.1	90.7	18.9	58.9	41.9	71.1	**65.8**	**25.6**

Running had the highest average 1MTP extension. Stance phase for running was calculated to be 0.19 ± 0.03 s, with 1MTP extension occurring between 40 and 90% of stance phase. Thus, the mean rate of 1MTP extension was between 700 and 1,000 deg/s. This range of rates dictated the target angular rotation rate specified for the test fixture described below.

2.2. Testing Methods

2.2.1. Test Fixture and Instrumentation Design

The test fixture consisted of a rotating fixture (toe plate) and three stationary reaction platforms (foot plate, heel platform, and tibia-fibula attachment plate). Rotation of the toe plate was induced by a linear, pneumatic impactor. A transfer piston from the impactor displaced cables wrapped around the toe plate which converted the linear movement to rotation (*Figure 5*).

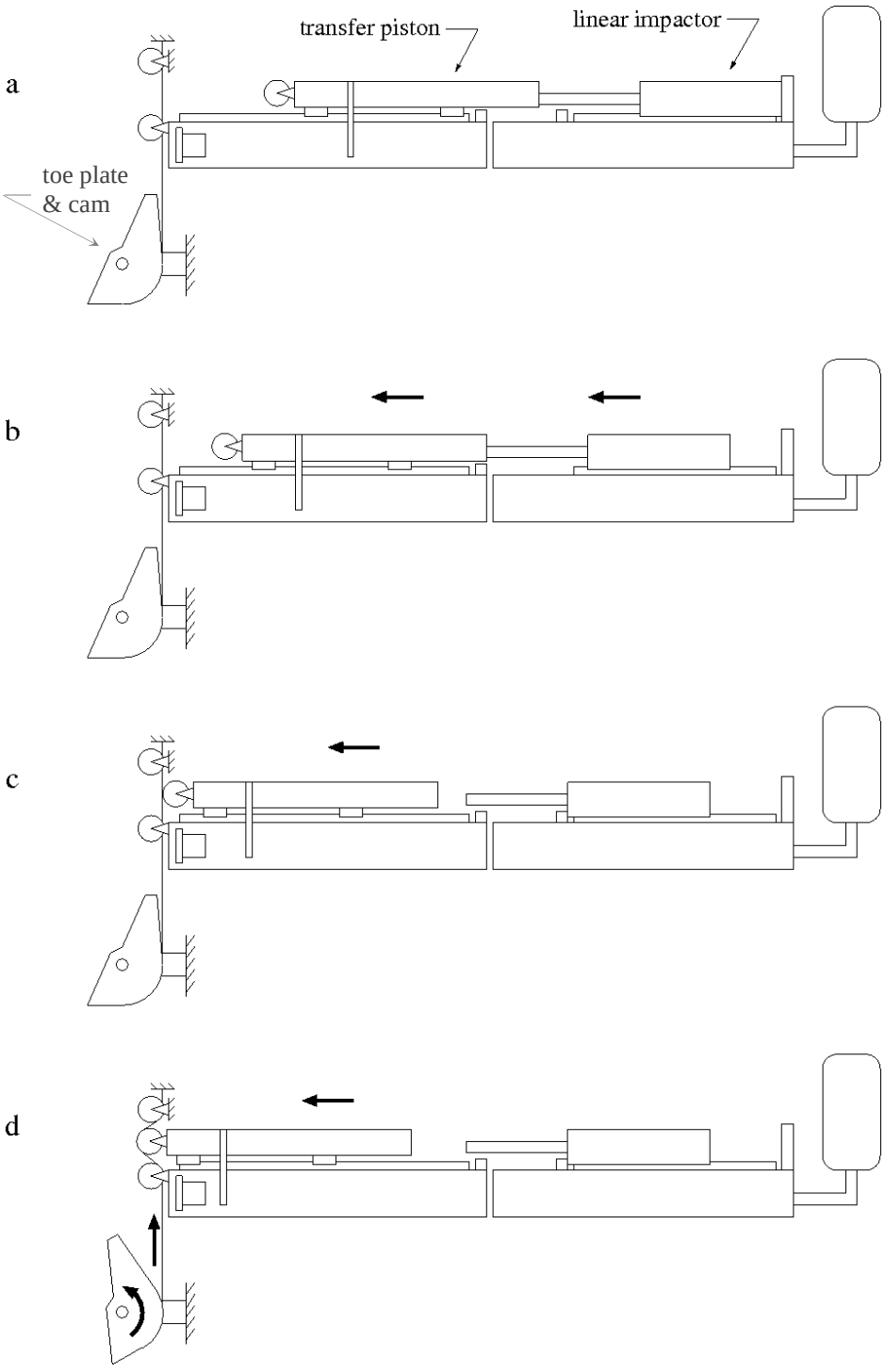

Figure 5 - visualization of impactor, transfer piston, cable, and toe plate/cam interaction.

Previous studies have shown that the instantaneous centers of rotation of the 1MTP joint move in space as a function of 1MTP extension; however, the instantaneous centers of 1MTP extension were always found within the first metatarsal head (Shereff 1986) (*Figure 6*). Because these instantaneous centers are closely grouped together, a fixed toe plate axis of rotation within the M1 head was deemed acceptable. An x-y-theta alignment table, at the tibia-fibular attachment to the test fixture, was included in the test fixture design to align the toe plate axis of rotation with the center of the M1 head for each specimen (*Figure 7*).

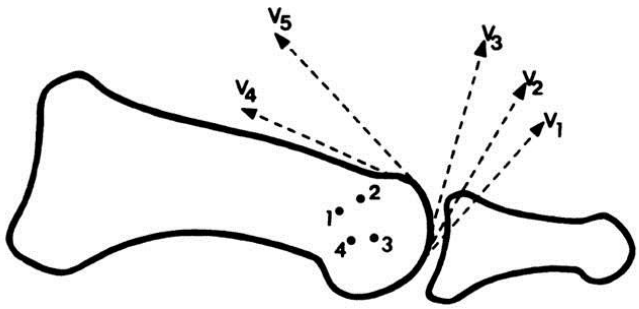

Figure 6 - instantaneous center of rotation during four positions of 1MTP extension. The dashed arrows represent surface-velocity vectors at each position. Used with permission (Shereff 1986).

In many biological materials the injury tolerance depends on rate of loading (e.g. Noyes et al. 1974, Woo et al. 1990). Unfortunately, the rate of loading when 1MTP sprain occurs has not been documented. In the absence of that information, the peak angular rates measured in the MARL performance tests were used as a conservatively low estimate of the rate present when injuries occur in the field. The test fixture was therefore designed to target an angular rate of 800 – 1200 deg/s. This was accomplished

by controlling the linear speed of the transfer piston, and the subsequent rotation of the toe plate, though adjusting the launch pressure of the pneumatic impactor. Because the instant of injury was not anticipated to be apparent during testing, prescribing the magnitude of rotation for each test was necessary for the analysis of doubly-censored data. The rotation magnitude was controlled by limiting the transfer piston's travel and by restricting the toe plate's rotation. Honeycomb blocks of varying thicknesses were used for this purpose. To avoid an impact to the 1MTP joint by the toe plate at the start of the test, pre-test tension was applied to the FHL to seat the hallux on the toe plate. A constant-force spring was used in series with a cam clamp attached to the FHL tendon to ensure this initial contact between the hallux and toe plate. The impactor was sufficiently massive (91 kg) such that its motion could be assumed independent of the characteristics or presence of the loaded foot.

Engineering parameters were recorded during testing though the use of load cells, accelerometers, angular rate sensors, a pressure mat, and motion capture methods (*Figure 7*) (Appendix A). Each of the loading and reaction platforms (toe, foot, heel, and tibial-fibula) recorded reaction forces through a six-axis load cell. A pressure mat (TekScan, F-Scan Hoof Sensor Model 3200; South Boston, MA, USA) recorded the center of pressure and ratio of forces through the hallux as compared to the other digits on the toe plate. A single-axis load cell was used in series with the constant force spring that loaded the FHL. Angular rate sensors were used to record toe plate motion; a linear accelerometer recorded transfer piston motion. A motion-capture system (Vicon; Centennial, CO, USA) was used to record the position of several markers attached to the test fixture and

the test specimen. Load cell, angular rate sensor, and linear accelerometer data were sampled at 10,000 Hz using a 36 channel TDAS Pro data acquisition system (Diversified Technical Systems, Inc.; Seal Beach, CA, USA). Pressure mat and motion-capture data were sampled at 1,000 Hz.

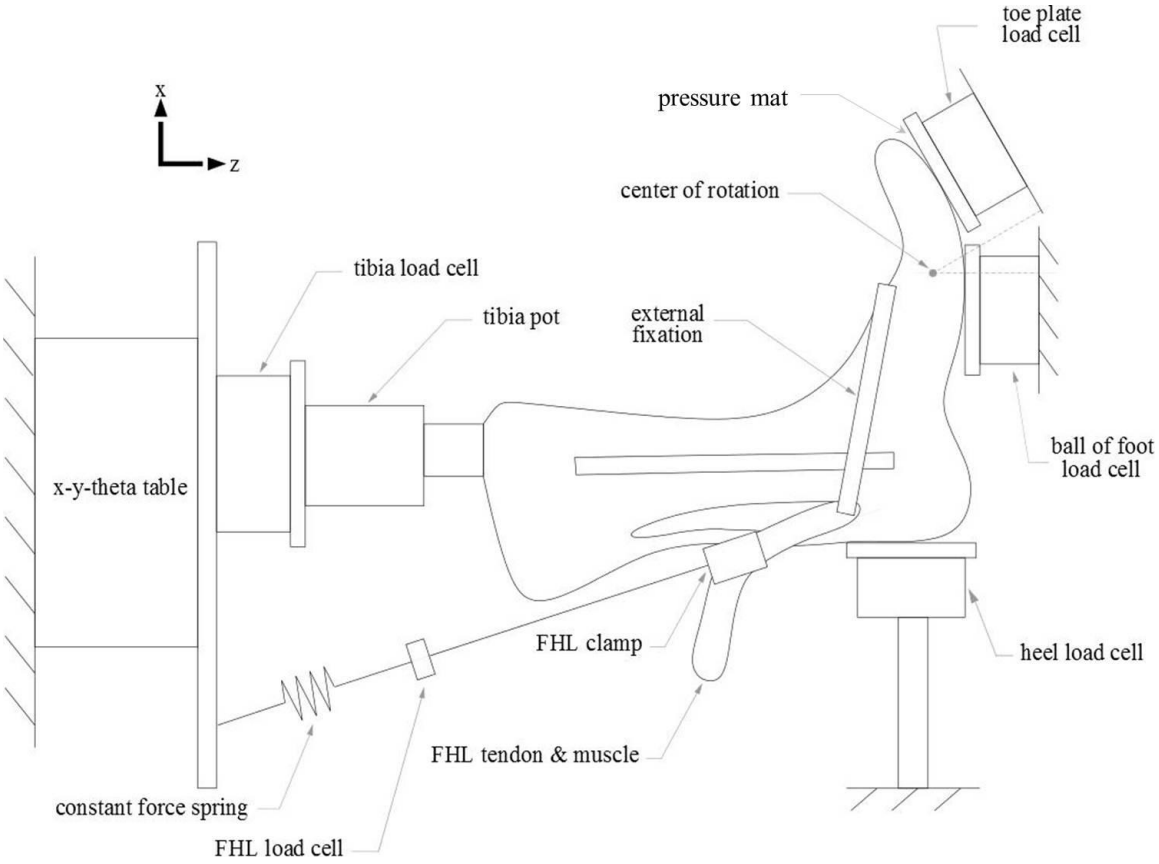

Figure 7 – schematic of test instrumentation. The cam and honeycomb cylinders are removed for visualization purposes. The pressure mat and motion-capture markers are not shown.

2.2.2. Specimen Preparation

During preparation, specimens were transected in the proximal third of the tibia/fibula. The 10 cm immediately adjacent to this cut were cleaned of all soft tissue

and potted using FastCast R802 (Goldenwest; Cedar Ridge, CA). The FHL was then exposed at the tarsal tunnel. Gauze was sutured to the proximal 15 cm of FHL muscle and tendon to aid the cam clamp during pre-test loading. External fixation (Synthes Corp; West Chester, PA, USA) was then applied to the foot to eliminate ankle compliance during testing (*Figure 8*). Two Steinmann pins were drilled into the tibia, approximately halfway along the bone. Two additional Steinmann pins were drilled into the medial aspect of the first metatarsal. These sets of pins were connected by carbon rods and clamped into place. The ankle of each specimen was set in a neutral position. The use of a consistent angle minimized injury tolerance variability introduced by variations in Hick's Windlass mechanism.

Figure 8 - external fixation eliminating hind-foot compliance.

Motion-capture arrays of four markers each were rigidly attached to the proximal phalanx, the first metatarsal, and the calcaneus (*Figure 9*). Each array was attached with two screws into bone. Due to space limitations, the first metatarsal array was attached

via the Steinmann pins used for external fixation. As these pins were rigidly attached to bone, this placement was deemed acceptable.

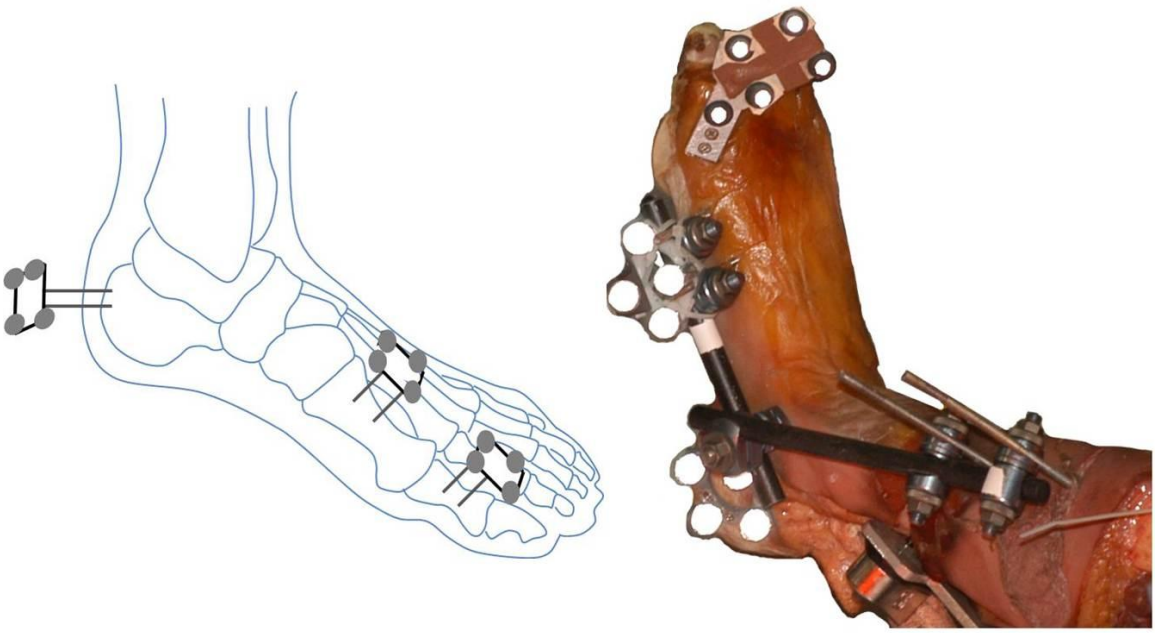

Figure 9 - motion-capture markers used during the test series.

Pre-test computed topography (CT) images were used to identify placement of the Steinmann pins and motion-capture arrays. These images also established that there was no observable pre-test injury to each specimen.

2.2.3. Test Procedure

Immediately prior to testing, the specimen was attached to the test fixture at the tibia-fibula through an alignment table. The specimen was then adjusted so that the metatarsal heads rested on the foot plate and the center of the 1MTP joint was aligned with the toe plate rotation axis. The cam cleat was attached to the gauze-wrapped section of the FHL tendon and used as the point of application of tension from the constant-force

spring. A pre-test data capture confirmed that the specimen was in contact with the toe and foot plates and that the FHL was loaded to approximately 40 N.

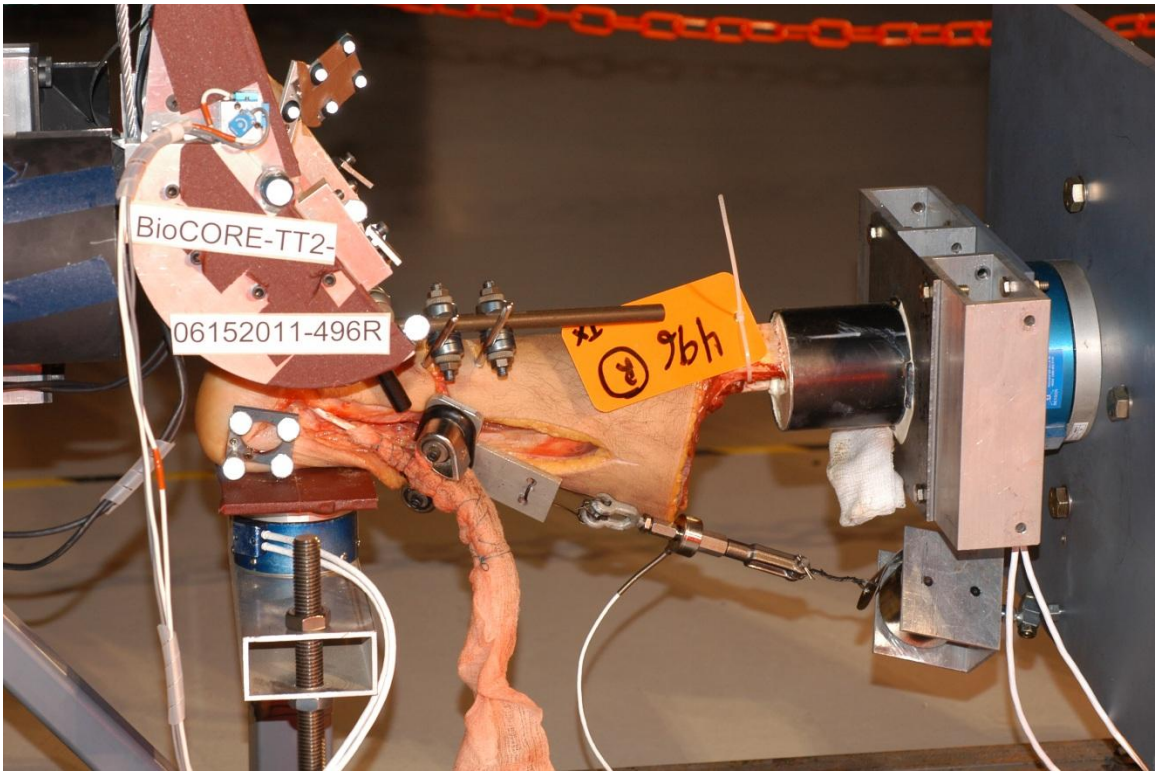

Figure 10 - specimen in the test fixture with FHL tension applied. The cam cleat and constant force spring are shown attached to the gauze-wrapped section of tendon and muscle.

Testing was conducted at pre-determined rotation rates and maximum extension angles. Each specimen was rotated to the prescribed amount and removed from the test fixture.

2.2.4. Injury Diagnosis

Post-test CT ensured that the motion-capture arrays remained fixed to bone and that no fractures were created during testing. Following post-test CT, each specimen was

dissected to assess injury. A foot and ankle surgeon or a physician familiar with the injury conducted each necropsy. Injury was defined as a visible tear in the plantar plate. Attenuation or stretching of the ligament without acute rupture was observed and documented, but this was deemed a subjective analysis not repeatable between specimens. Because attenuation was not able to be quantified, it was not considered to be an injury for the purposes of injury risk function development.

2.2.5. Motion-Capture Analysis

Motion-capture analysis began with segmenting the CT scan of each foot into three structures, including images of the associated motion-capture markers: the hind-foot (calcaneus and tarsal bones), the first metatarsal, and the proximal phalanx of the hallux (*Figure 11*). Segmentation was completed using Mimics software (Materialise; Leuven, Belgium). A separate coordinate system was imposed on the first metatarsal and the proximal phalanx. The x-axis of the first metatarsal connected the centers of the proximal and distal joint surfaces of the bone. The first metatarsal y-axis was parallel to a line connecting the most plantar points of the sesamoid bones. The z-axis was orthogonal. The origin was the center of the base of the first metatarsal, identified as the center of the concave proximal joint surface determined through visual inspection. Similarly, the hallux coordinate system was defined with an origin at the center of the proximal joint surface, with the x-axis linking the centers of the proximal and distal joint surfaces, the y-axis parallel to the plantar surface of the distal head, and the z-axis orthogonal. The location of each motion tracking marker array ($\boldsymbol{\eta}$) was determined within the defined coordinate system on bone ($\boldsymbol{\beta}$) using a transformation matrix ($\mathbf{T}$):

$$\boldsymbol{\beta} = \mathbf{T}\boldsymbol{\eta} \quad (1)$$

This transformation was completed using Magics software (Materialise; Leuven, Belgium). OpenSim (version 2.4; http://opensim.stanford.edu) was used to describe six degree of freedom (6DoF) motion of the 1MTP joint using a mathematically consistent coordinate transform. 1MTP extension angle was defined as the angle between the x-axis of the metatarsal coordinate system and the x-axis of the hallux coordinate system. Zero-angle (0°) was defined as the alignment of the x-axis of the hallux coordinate system with the x-axis of the metatarsal coordinate system.

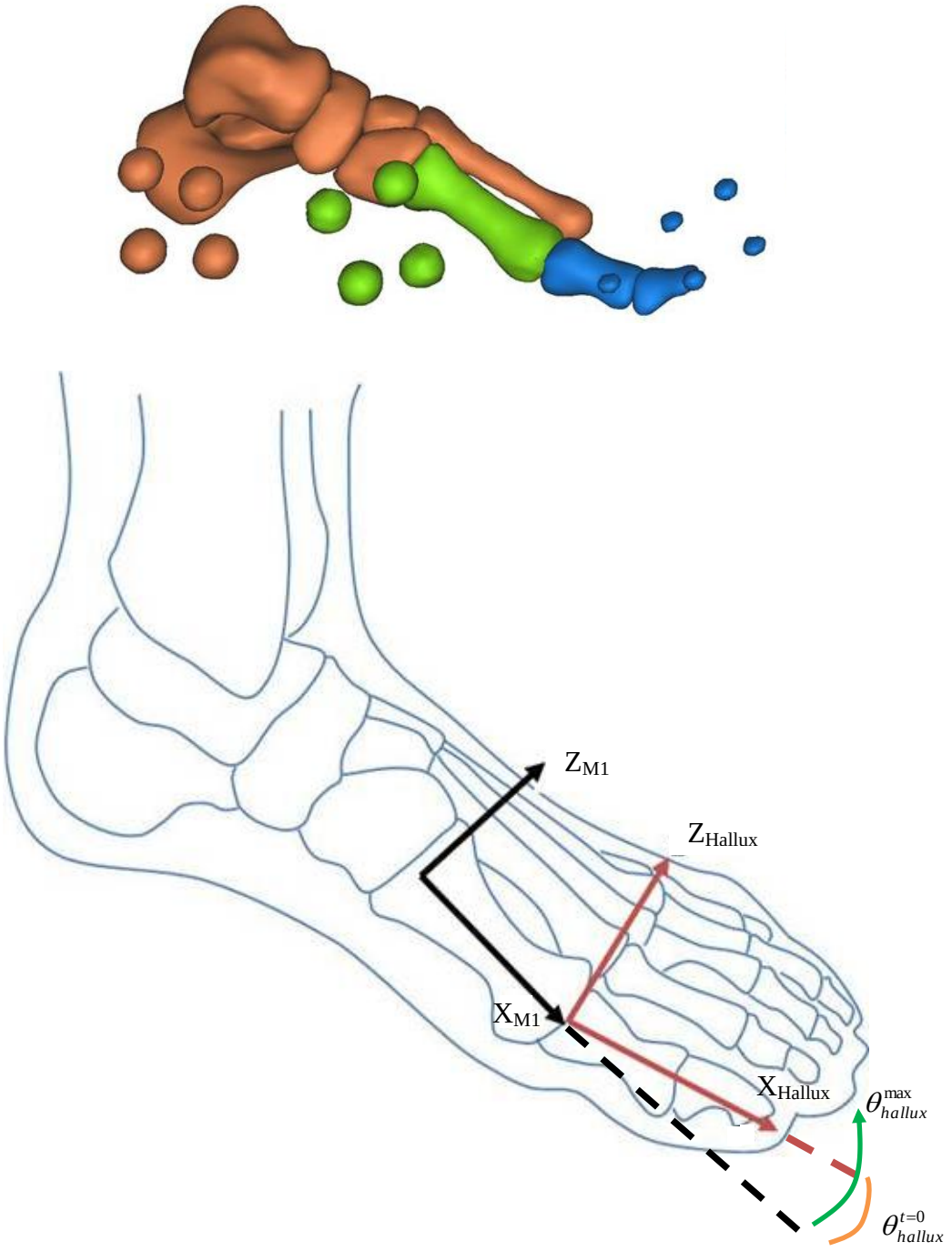

Figure 11 - extracted three-dimensional surface of bones and reflective markers from CT images. The three colors represent three structures: hind-foot in orange, first metatarsal in green, and first proximal and distal phalanx in blue. Also, a line drawing of bones of the foot with applied coordinate systems from 6DoF analysis of motion.

2.2.6. Variable Definition and Computation

Kinematic and kinetic variables were recorded during testing. An iterative process of filter adjustment suggested that a CFC 500 filter was appropriate (Figure 12). All load cell, accelerometer, and angular rate sensor data were subsequently filtered at this level.

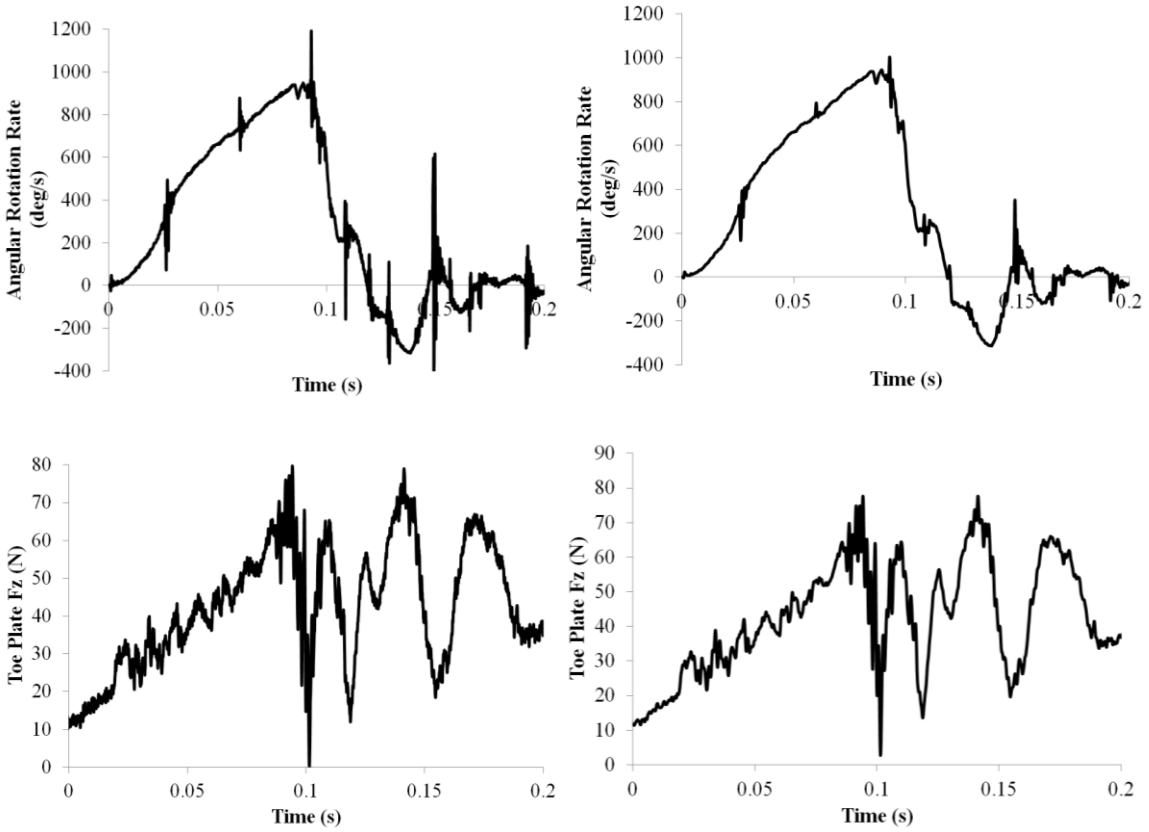

Figure 12 - examples of data pre- and post- filtering. The plots on the left are unfiltered data while the plots on the right are data with a 500 CFC filter applied for specimen 496L.

The maximum toe plate angle (θ_{tp}) was determined by integration of the angular rate sensor data. Three variables were taken from motion-capture analysis: the toe angle at the start of test ($\theta_{hallux}^{t=0}$), the absolute maximum hallux extension angle, and the

maximum change in the hallux extension angle. The maximum hallux extension angle ($\theta_{hallux}^{\max}$) was defined as the greatest angle achieved during testing, with reference to the zero-angle, 0°. The maximum change in the hallux extension angle ($\Delta\theta_{hallux}^{\max}$) was calculated as the difference between the maximum angle and the angle at the start of the test (t=0).

The moment at the 1MTP joint was calculated using the toe plate load cell, pressure mat, and motion-capture data. During post-test data analysis, the pressure mat data was analyzed using software provided by TekScan. With this software, a region of interest (ROI) was created around the hallux for each specimen (*Figure 13*). The pressure mat was not calibrated to measure absolute load, so these data were only to apportion the measured toe-plate force among the digits in contact with the mat. The ratio, α, of force through the ROI (F_{ROI}) as compared to the force through the entire pressure mat (F_{Total}) was calculated for each time step:

$$\frac{F_{ROI}}{F_{Total}} = \alpha \tag{2}$$

The force through the hallux, **F**, was calculated by multiplying α by toe plate load cell data. Instantaneous moment arms for **F** were determined at each time step through motion-capture analysis. During pre-test Vicon calibration, a linear probe of motion-capture markers defined known positions on the pressure mat. These positions were then used to develop a transformation matrix, **λ**, from the pressure mat coordinate system to the motion-capture coordinate system. Post-test, the location of the center of pressure within the ROI was determined at each time step using the TekScan software, in pressure

mat coordinates, and then transformed, using **λ**, into the motion-capture coordinate system. Similarly, the position of the 1MJP joint center was calculated using OpenSim for each time step, in the motion-capture coordinate system. From this, a vector from the 1MTP joint center to the hallux center of pressure, **d**, was defined. Moment was then calculated as

$$\mathbf{M} = \mathbf{F} \times \mathbf{d} \tag{3}$$

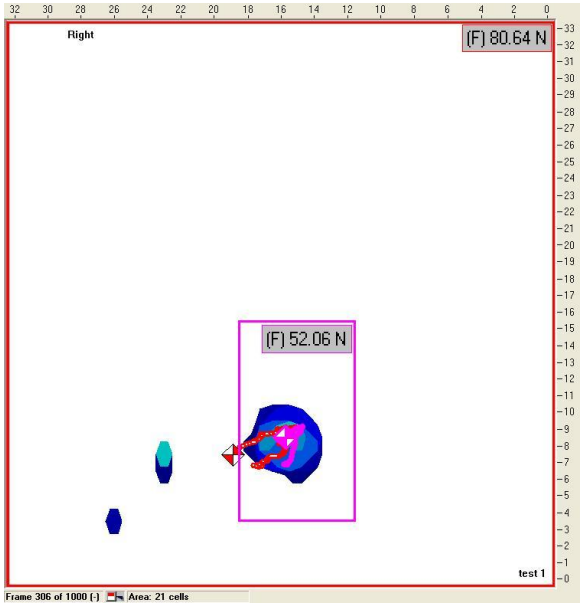

*Figure 13 - screen capture of TekScan software used in processing the pressure mat data. The contacts of rays 1 - 3 with the mat are visible in this image. The contact of the hallux (first ray) is contained within the purple box as the region of interest. The pressure mat measured only proportionate load, not absolute load; In the test shown, 64% of the force is through the hallux: (52.06/80.64)*100 = 64%.*

Though the test fixture was designed to reduce impact vibration when braking the toe plate rotation, the rapid deceleration nonetheless caused a "ringing" in the load cell data and spikes in the angular rate sensor. This noise resulted from motion of the test

fixture and did not act upon the specimen. As such, the joint moment was calculated only up to the time of contact between the toe plate and the honeycomb limiting its rotation. The onset of noise was defined as any change greater than or equal to 15 N between two consecutive time steps of load cell data. Moment calculation was only performed for the 15 specimens included in the final risk analysis. Similarly, maximum angular rate was recorded immediately preceding noise, defined as an interval of 75 deg/s between successive data points.

2.3. Results

Twenty-one male lower extremities, 10 right and 11 left, were tested with approval from the University of Virginia Center for Applied Biomechanics Oversight Committee and the UVA Institutional Biosafety Committee (*Table 3*). The donor's age at the time of death ranged from 18 – 69 years, with an average of 46.5 years. Specimens were tested to varying degrees of hyperextension.

Table 3 - tested specimen information. Height and weight information was not available for specimen 411.

Subject #	Age (years)	Height (cm)	Weight (kg)
400	53	182	145
411	60		
416	69	191	51
486	53	170	68
487	27	170	73
488	40	165	64
490	52	178	64
492	66	178	70
493	63	170	82
495	18	178	75
496	31	170	73

Pre-test CT images revealed that no boney injuries were created during specimen preparation. Likewise, post-test CT images confirmed that no bony injuries were created at any of the external fixation sites, the tibia-fibula potting interface, or at the motion-capture array attachment sites.

During post-test necropsy, injuries were observed in 11 of the specimens (*Table 4*). The remaining nine specimens exhibited no tearing of the plantar plate. The observed injury was a tear of the plantar plate immediately distal to the medial sesamoids (*Figure 14*). These tears occurred partially through the thickness of the plantar plate, originating on the deep surface, and ranged from 0.25 – 1.5 times the width of a sesamoid. In two specimens, the soft tissue between sections of a bi-partite sesamoid was

either attenuated or torn as observed in post-test necropsy. The attenuation occurred in addition to tears in the plantar plate of these specimens. Attenuation was also commonly noted in the joint capsule of the specimens with torn plantar plates. Physicians performing the necropsy confirmed that the patterns of injury were consistent with their clinical experience.

Arthritis or degradation of the 1MTP joint articulating surface was noted in several of the specimens during necropsy. In consultation with the physicians performing the dissection, only specimen 493 L was deemed to have advanced degradation, joint calcification, of the joint surface to warrant exclusion from the data set. As a result, the contralateral limb was never tested and further data analysis on this specimen was not performed.

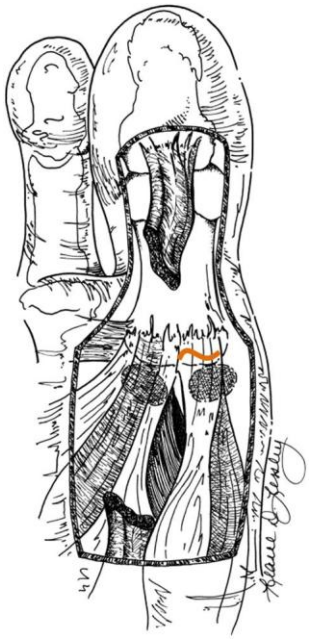

Figure 14 - depiction of tear location on anatomy.

Table 4 - injury information for tested specimens.

Test #	Specimen #	Description	Injury [Y/N]
1	416L	lateral sesamo-phalangeal ligament tear, partial tear of dorso-lateral plantar plate, laxity/stretch of the MCL	Y
2	486L	Medial capsule laxity, some laxity of MCL	N
3	488L	partially torn MCL, partial tear of medial sesamo-phalangeal ligament, partial tear of lateral platar plate	Y
4	411R	Complete tear of medial capsule, medial-central plate plate tear, osteophytes/arthritis	Y
5	487R	congenital medial bipartite sesamoid, MCL laxity	N
6	416R	-	N
7	486R	medial plantar plate tear	Y
8	488R	-	N
9	411L	Tear of medial-distal plantar plate, arthritis with medial sesamoid degradation	Y
10	487L	Medial plantar plate tear, lateral sesamoid plantar plate separation from an intersesamoid plantar plate	Y
11	400R	75% tear of plantar plate, medial sesamoid retracted, attenuation of sesamo-phalangeal ligaments, MCL avulsed from metatarsal head, arthritis, condral injury to metatarsal head, chondral injury to lateral sesamoid, osteophyte on proximal aspect of medial sesamoid	Y
12	490R	50% tear of medial sesamo-phalangeal, complete tear of plantar plate, chondral damage to lateral metatarsal head	Y
13	496R	Partial tear of medial sesamo-phalangeal ligament	Y
14	493L	Attenuation of MCL, calcification around sesamoids, partial tear of lateral and complete tear of medial sesamo-phalangeal ligament	Y
15	495L	50% tear of medial sesamo-phalangeal ligament	Y
16	400L	Arthritis, calcification of sesamoids and metatarsal head, partial (25%) superficial tear of medial platar plate	Y
17	490L	Chondral injury on metatarsal head, osteophyte on lateral sesamoid	N
18	496L	-	N
19	492L	-	N
20	492R	-	N
21	495R	-	N

Analyzed data are reported in *Table 5*. Maximum values of **M**, θ_{tp}, θ_{hallux}^{max}, $\Delta\theta_{hallux}^{max}$ are shown as well as specimen number, specimen age at time of death, foot aspect (right/left), $\theta_{hallux}^{t=0}$, and angular rotation rate. In figures, Moment refers to **M**, Toe Plate Rotation Angle refers to θ_{tp}, and the maximum value of 1MTP Extension Angle is equivalent to θ_{hallux}^{max}. Typical data traces for injured and non-injured specimens are shown in *Figure 14* and *Figure 15* while Appendix B contains plots for each specimen included in the final data analysis.

At initiation of toe plate rotation, the pre-loading through the FHL can be seen in the hallux moment. The data tabulated for $\theta_{hallux}^{t=0}$ reflect that the initial hallux angle was not zero. As the toe plate rotated at the prescribed rate, hallux angle and moment increased up to the point at which rotation was arrested. Values of up to 125° of toe plate rotation and 113° of 1MTP extension were generated, and hallux moment as great as 16 Nm were calculated. The sudden arrest of motion is seen in the spikes in the angular rotation rate plots.

Instant of injury could not be determined from the data. Average θ_{tp}, θ_{hallux}^{max}, and $\Delta\theta_{hallux}^{max}$, and **M** were greater in the injured group compared to the non-injured group of specimens. There was a 2% difference, 21 deg/s, in rotation rate between the injured and non-injured groups. Age was older in the non-injured group by six years. Immediately prior to testing, the FHL cam clamp fell off of one specimen, 416 L. The force in the FHL increased monotonically with 1MTP extension in all other cases.

Table 5 - maximum values for key variables. Moment has been calculated only for those specimens included in the final analysis (see section 3.3).

Specimen	Foot Aspect (L/R)	Age (years)	θ_{tp} (deg)	$\theta_{hallux}^{t=0}$ (deg)	$\theta_{hallux}^{\max}$ (deg)	$\Delta\theta_{hallux}^{\max}$ (deg)	Rotation Rate (deg/s)	Moment (Nm)	Injury (Y/N)
400	L	53	56	0	56	56	1000	-	Y
400	R	53	72	53	91	38	1300	4	Y
411	L	60	74	39	89	51	900	9	Y
411	R	60	95	18	103	68	1000	-	Y
416	L	69	125	27	113	85	1450	-	Y
416	R	69	75	25	83	58	1125	3	N
486	L	53	90	37	92	74	1500	10	N
486	R	53	87	18	72	57	900	15	Y
487	L	27	87	27	85	59	850	14	Y
487	R	27	72	4	44	39	1000	5	N
488	L	40	90	37	86	49	1200	5	Y
488	R	40	75	47	91	44	1000	-	N
490	L	52	62	40	78	37	1025	4	N
490	R	52	70	29	86	57	1100	4	Y
492	L	66	62	29	75	46	1100	4	N
492	R	66	44	34	59	25	700	3	N
493	L	63	Advanced arthritis – data not tabulated						Y
495	L	18	67	24	87	63	900	-	Y
495	R	18	54	27	53	25	900	3	N
496	L	31	60	30	67	37	950	4	N
496	R	31	68	28	79	51	1000	4	Y
Average of injured		45	80	27	86	57	1054	7	
Average of non-injured		51	67	30	73	43	1033	4	

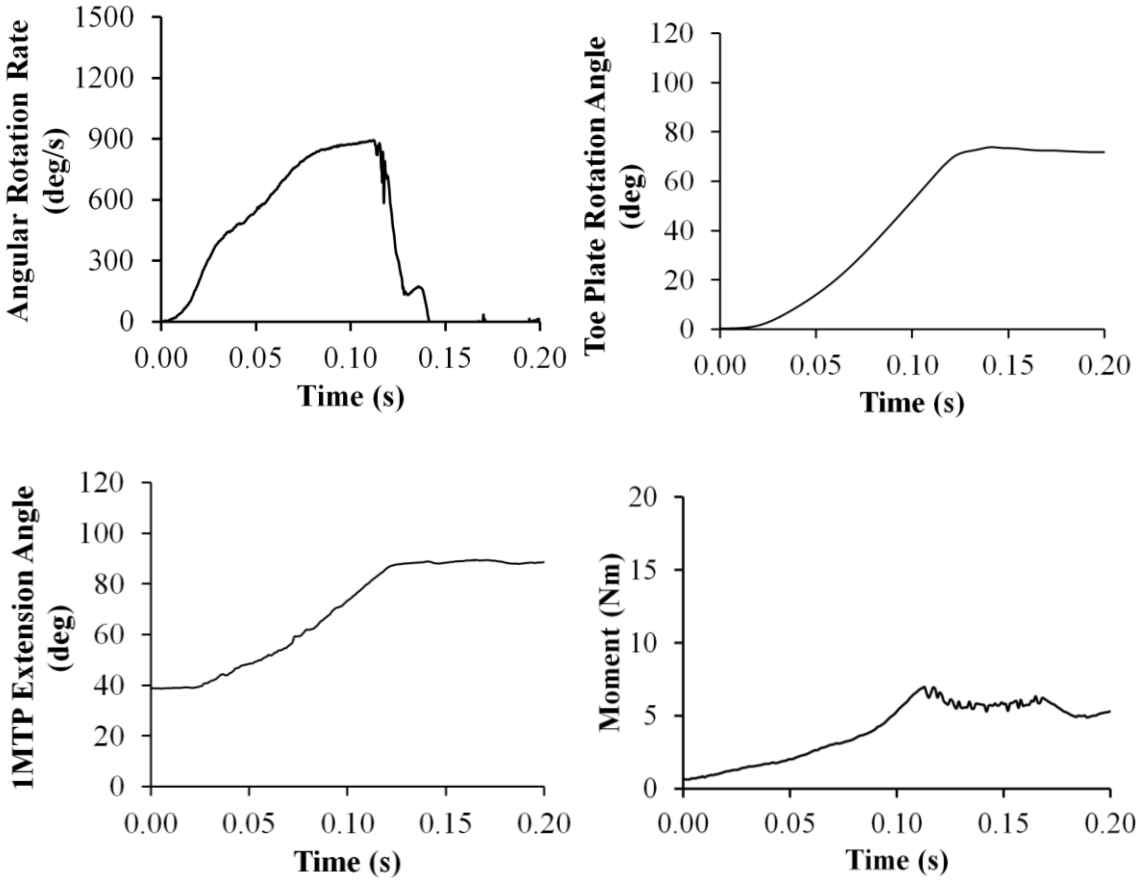

Figure 15 - representative data traces of an injured specimen (411L).

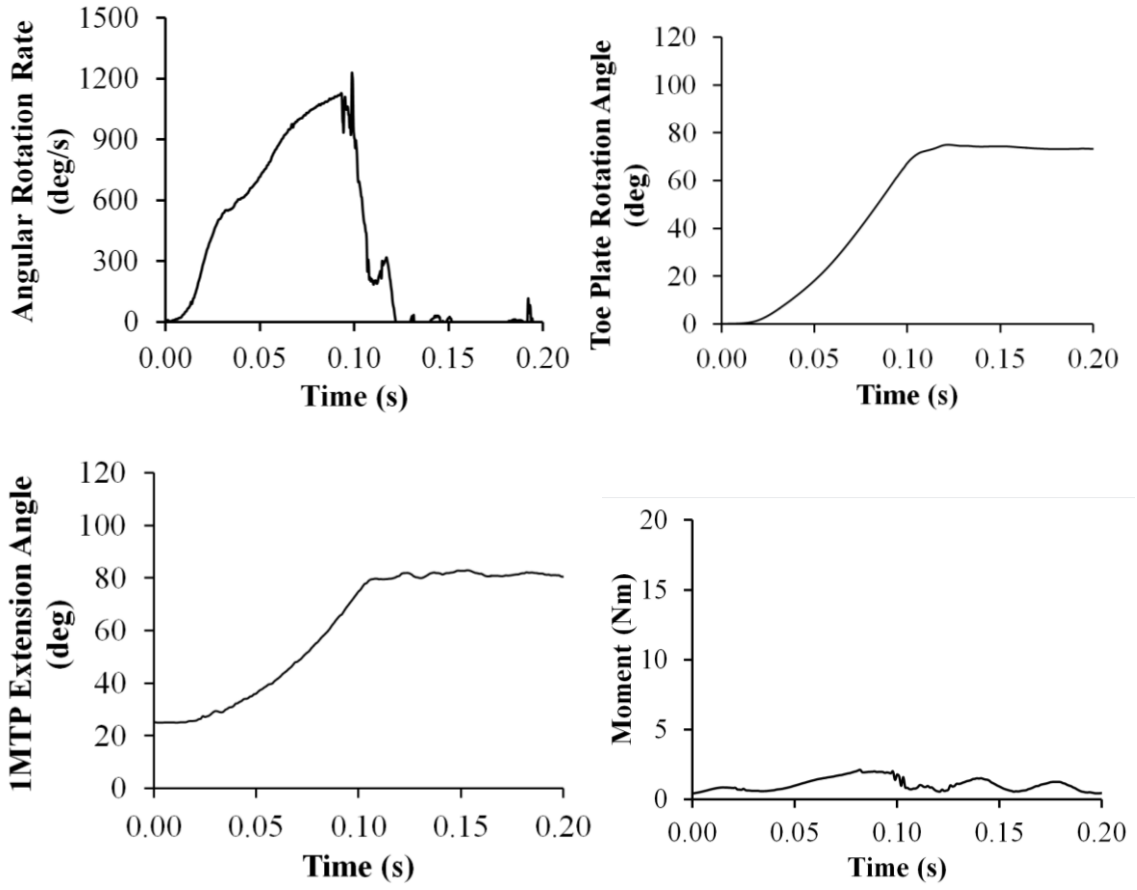

Figure 16 - representative data traces of a non-injured specimen (416 R).

2.4. Discussion

This study was the first to produce clinically-relevant 1MTP sprains *in vitro* using cadaver specimens through hyperextension of the joint. Though many sources have suggested hyperextension as a mechanism of 1MTP sprain (e.g. Bowers and Martin 1976, Rodeo et al. 1990, Clanton et al. 1986, Coker et al. 1978), the only previously published

test series which evaluated this mechanism reported injuries inconsistent with case studies of 1MTP sprain (Preiskorn et al. 1995). The test fixture design and testing parameters (e.g. rotation rate, initial degree of extension) were informed by the results of an athlete performance study. Hyperextension was shown to be an injury mechanism of 1MTP sprain by producing tears in the plantar plate. Clinicians familiar with the treatment of this injury confirmed that the pattern of soft tissue trauma generated in these experiments represents what occurs in the field. During these trials, non-injurious extension specimens were also created in anticipation of developing injury risk functions.

1MTP sprains are not associated with marked fractures (Bowers and Martin 1976), and the typical method of diagnosis of 1MTP sprain in an athlete is unsuitable for use in PMHS specimens (McCormick and Anderson 2009, Clanton et al. 1986, Graves et al. 1991, Allen et al. 2004). As a result, clinicians performed post-test necropsy for the tests herein. In order to standardize the diagnosis, a visible tear was required for a specimen to be considered injured. Though this method assured a precise definition of injury, it omitted less severe but still damaged cases. For example, attenuation of the plantar plate, which was not deemed an injury, is a possible cause of pain in an athlete and may require time away from sports. Indications of injury such as pain, ecchymosis and swelling, could lead the athlete with an attenuated plantar plate to be diagnosed with 1MTP sprain based upon established grading systems (Clanton et al. 1986 and McCormick and Anderson 2009); however, as the PMHS specimens would not exhibit these physiological symptoms of injury, the athlete with an attenuated ligament would not have been considered injured in this study. The injuries diagnosed were the most

severe form of sprain. As a result, any injury criteria informed by this study will apply to severe 1MTP sprains, and less severe injury may occur at a stimulus less than described in this study.

Injury risk functions will be developed in the next chapter based upon the peak values of predictive variables. The filters chosen for processing data affect peak values, which in turn affect subsequent analysis and development of injury risk criteria. There is no published guide which directly indicates which filters should be used for cadaver injury testing. The filters used for data analysis were chosen to retain signal while eliminating noise. Additionally, both maximum moment and maximum angular rate were determined before the onset of test fixture vibrations, which helped mitigate the effects of filtering. The data used as a peak value was collected at a time before filtering would have had the greatest effect. Furthermore, the inherent variations in biological tissue, as demonstrated in the confidence intervals in the injury risk function (see section 3.3: *Figure 19* and *Figure 21*), represent a greater variability than filtering effects when data is examined before transient vibrations.

Toe plate rotation was induced by means of a pneumatic impactor. Over the course of a test day, a consistent firing pressure at the impactor would result in different toe plate rotation rates throughout the test series. As a result, the test specimens experienced a range of rotation rates from 700 – 1500 deg/s. Though strain rate has been shown to have an effect on failure properties of biological tissue, variation in rate needs to be greater than what was used here to have a significant effect on failure (e.g. Noyes et al. 1974, Woo et al. 1990). Also, this range of rotation rates was deemed acceptable as

none went below rates observed during the performance tests. Evaluation of rotation rate will be evaluated as a possible confounding variable in the next chapter. If toe plate rotation rate is predictive of injury, further testing will be necessary.

The test specimens were limited to the available supply at the Center for Applied Biomechanics. Though effort was made to use younger specimens, specimens as old as 69 years were included in this test series. One potential limitation of this study is, therefore, the presence of arthritis and other degenerative conditions associated with age. A specimen with arthritis may require more force, and, as a result, a larger moment, to reach a given extension angle than a healthy joint. Also, though no degradation of the plantar plate was noted, non-visible soft tissue defects may have predisposed specimens to injury. Soft tissue weakness as a result of specimen age may lower the angle at which injury occurs, thus creating a more conservative injury criterion. Thus the conclusion of this study applies to this study population. Application to another population, such as elite athletes, requires caution.

This test series evaluated 1MTP sprain as an acute injury only. This is clearly appropriate when considering situations such as one player in contact with another; however, 1MTP sprains have also been reported as a result of routine exercise and without athlete recollection of a distinct injury event (Mullis and Miller 1980, Kubitz 2003, Prieskorn 1995). Thus, in addition to acute injury, 1MTP sprain may also occur as a result of repetitive, sub-catastrophic damage. Testing for chronic injury was out of the scope of this study. Chronic loading, or repetitive microtrauma, may decrease the angle

or load at which injury occurs. In the case of chronic injury, the peak values presented herein should be treated as maximum values for injury tolerance.

This study confirmed hyperextension as a mechanism for severe, acute 1MTP sprain. Physicians experienced with this injury in athletes confirmed that the pattern of tears was consistent with trauma in the field. Data tabulated from these experiments can now be correlated with outcome of injury to develop injury criteria.

3. Injury Criteria

The goal of this task is to utilize statistical tools to describe and evaluate the *in vitro* cadaver testing results. This analysis was completed in three stages. First, a final data set was developed based upon defined exclusion criteria. Second, variables recorded during testing were assessed based upon their ability to predict an injurious outcome. Third, the most discriminating variables were used to describe risk of injury using survival analysis methods.

3.1. Background

An injury risk function is a statistical tool used to relate a quantifiable parameter to the probability of injury. Development of these risk functions is complicated in many biomechanical applications because it is oftentimes impossible to pinpoint the exact instant of injury. Censored data is the term used to indicate data with incomplete failure information (Hosmer and Lemeshow 1999). For example, if an applied force does not result in an injury, the peak force is a left censored data point because the magnitude of force that would have been required to generate injury is unknown. In other words, injury occurs at some unknown point past the maximum measured value. Conversely, a right censored data point is created when injury is generated at some unknown point less than the maximum recorded value. Injury biomechanics data are frequently doubly-censored, indicating that injured specimens are right censored and non-injured specimens are left-censored (DiDomenico and Nusholtz 2003). Survival analysis is a method by which censored data are formed into injury risk functions. Originally, this technique was

developed to describe time to death for medical research; however, any parameter relating to failure, not just time, may be used as the independent variable (Funk et al. 2002).

The two main components of survival analysis are the survival function and the hazard function. The survival function, S(x), is the probability that injury occurs at a stimulus higher than a given value, x. Funk (2000) states that the survival function is more precisely the probability that the stimulus resulting in injury, X, is greater than the given stimulus, x. A probability density function, f(x), relates the distribution of injury stimuli, X, to the population. The cumulative density function, F(x), is obtained by integrating the probability density function. The survival function and the cumulative density function are related by

$$S(x) = P(X \geq x) = 1 - F(x) = 1 - \int_0^f f(x)dx \tag{4}$$

The hazard function, on the other hand, is the probability that an injury occurs at a given stimulus, conditional on it having been un-injured to that point (Funk 2000). It can be shown that the cumulative hazard, H(x), is related to the survival function through

$$H(x) = -\ln S(x) \tag{5}$$

Typically, in injury biomechanics, hazard functions are reported as injury risk plots with 95% confidence intervals.

Along with the ability to use censored data, survival analysis is appropriate to use with injury biomechanics due to non-normality of the data. Both parametric (e.g. normal, log-normal, Weibull) and non-parametric forms are available for use with survival analysis. Of the non-parametric forms, the Consistent Threshold method is commonly

applied to injury biomechanics (Nusholtz and Mosier 1999). However, because parametric forms result in continuous functions, this method is generally preferred for a final form of risk analysis (Kent and Funk 2004). Any parametric form may be used to develop a risk function. Due to the small data sets typical in injury biomechanics research, parametric form has not been shown to have a large effect on the validity of a resultant injury risk function (Kent and Funk 2004). Weibull distributions are often used when a parametric form is desired because this distribution predicts a 0% chance of injury when stimulus is non-existent.

3.2. Methodology

The group of tested specimens was examined for outliers based upon assessment of test conditions. Because this sample is small, careful assessment of the data was needed. Data points were examined for any irregularities in testing protocol, data processing, or motion-capture analysis. Possible exclusion criteria included improper placement of the specimen on the test fixture, test fixture failure, improper placement of motion-capture markers, obstruction of motion-capture cameras during test, unsuitable specimen condition, and improper necropsy methods. The final data set resulting from this step was used in all subsequent analyses.

The ability of nine tested variables to discriminate between injurious and non-injurious conditions was assessed using the Goodman-Kruskal Gamma (γ) and percent concordance. Concordance pairs tested specimens to assess if the model predicts a higher probability of injury for the injurious case than for the non-injurious case. If the model

did so, then the pair was labeled concordant. If the model did not correctly predict injury, the pair was considered discordant. The Goodman-Kruskal Gamma was defined by the difference in the number of concordant pairs, N_c, minus the number of discordance pairs, N_d, in a dataset, divided by the total number of pairs (Kent et al. 2008). Ties were neglected for this statistic

$$\gamma = \frac{N_c - N_d}{N_c + N_d} \tag{6}$$

Thus, γ varies from -1 to 1. A value of -1 suggests that the pair has the inverse relationship as compared to the modeled relationship. A value of zero indicates that the variable of interest has no predictive ability. Similarly, a value of 1 is indicative of perfect discrimination. This analysis was performed through a binary logistic regression routine in Minitab 16 (Minitab Inc.; State College, PA, USA). The regression also reported p-values on both the constant and variable being examined.

Survival analysis was then conducted on the most predictive variables. A non-parametric initial estimate using the Consistent Threshold method was performed in Excel 2012 (Microsoft Corp.; Redmond, WA, USA). This initial estimate was used to both evaluate applicability of each variable and to visually assess the choice of parametric form. The data were then through Minitab's survival analysis routines to a Weibull distribution. Many methods are available to estimate the shape and scale parameters which define a Weibull distribution. Though Minitab defaults to an ordinary least squares (LS) method, this program also supports a maximum likelihood (ML) routine for parametric estimation. Historically, because of its relative computational simplicity, LS methods have been used to estimate the shape and scale parameters of the

Weibull distribution. With the advent of computer-based statistical packages, more computationally-intense ML methods have become feasible. Studies (e.g. Genschel and Meeker 2010) have suggested that in the case of heavily censored data, the ML methods may estimate parameters more closely representative of the true distribution for all but samples containing only one or two failure points. Both routines will be used to formulate injury risk curves.

3.3. Results

Of the original 21 data points, six were excluded from the final data set (*Table 6*). One test (416 L) was removed due to text fixture failure (FHL cam cleat disengaged from tendon immediately pre-test), one test (493 L) was removed because of specimen condition (excessive calcification), and four tests (488 R, 411 R, 495 L, and 400 L) were removed due to motion-capture error.

Table 6 - specimens excluded from data analysis.

Test	**Specimen**	**Aspect [L/R]**	**Reasons for exclusion**
1	416	L	absence of FHL loading during testing
3	488	R	marker in joint space instead of in bone
4	411	R	only 2 markers visible on the hallux
14	493	L	gross calcification of MTP joint
15	495	L	marker array in distal phalanx instead of proximal phalanx
16	400	L	proximal phalanx array screw into skin only, not bone

The occurrence of injury is cross-plotted in *Figure 17* against the nine variables that were evaluated as potential predictors of injury. Maximum hallux angle and maximum moment were shown to have similar discriminating ability (*Table 7*).

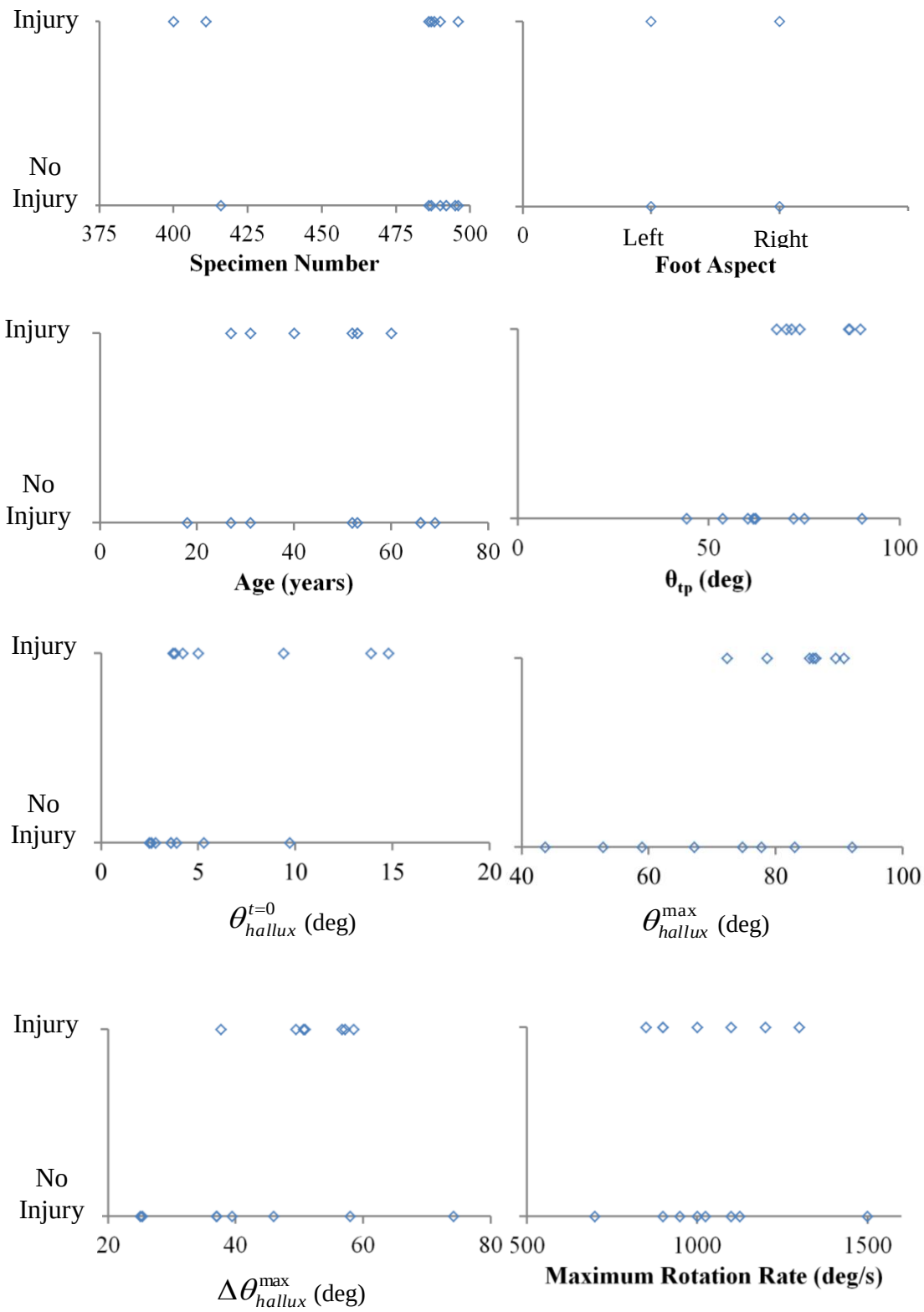
Injury
No Injury
375
400
425
450
475
500
Specimen Number
0
Left
Right
Foot Aspect
Injury
No Injury
0
20
40
60
80
Age (years)
0
50
100
θtp (deg)
Injury
No Injury
0
5
10
15
20
θ^t=0 hallux (deg)
40
60
80
100
θ^max hallux (deg)
Injury
No Injury
20
40
60
80
Δθ^max hallux (deg)
500
1000
1500
Maximum Rotation Rate (deg/s)

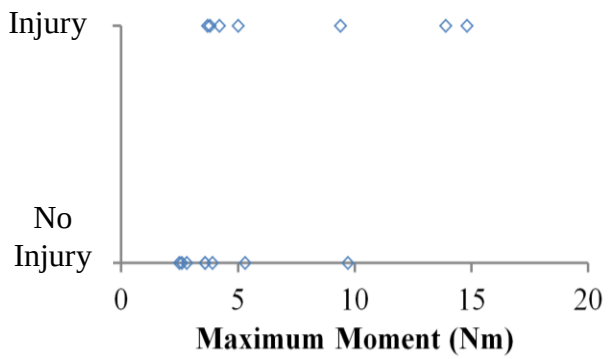

Figure 17 - injury plots for each variable. Each open diamond represents one tested specimen included in the final dataset.

Table 7 - assessment of variables.

Variable	Specimen Number	Aspect [R/L]	Age	θ_{tp}	$\theta_{hallux}^{t=0}$	θ_{hallux}^{max}	$\Delta\theta_{hallux}^{max}$	Max. Angular Rate	Max. Moment
Gamma	0.38	0.14	0.14	0.50	0.14	0.61	0.50	0.08	0.61
Concordance (Percent)	64.30	28.60	51.80	75.00	57.1	80.40	75.00	46.40	80.40
Discordance (Percent)	28.60	21.40	39.30	25.00	42.9	19.60	25.00	39.30	19.60
Ties (Percent)	7.10	50.00	8.90	0.00	0.00	0.00	0.00	14.30	0.00
P-value (constant)	0.37	0.71	0.83	0.24	0.40	0.09	0.10	0.10	0.12
P-value (variable)	0.36	0.78	0.75	0.25	0.42	0.09	0.09	0.10	0.13

Non-parametric injury risk functions are shown in *Figure 18* for θ_{hallux}^{max}, $\Delta\theta_{hallux}^{max}$ and maximum moment. Because the largest angles for θ_{hallux}^{max} and $\Delta\theta_{hallux}^{max}$ correspond to a non-injury point, the non-parametric function did not attain 100% risk of injury.

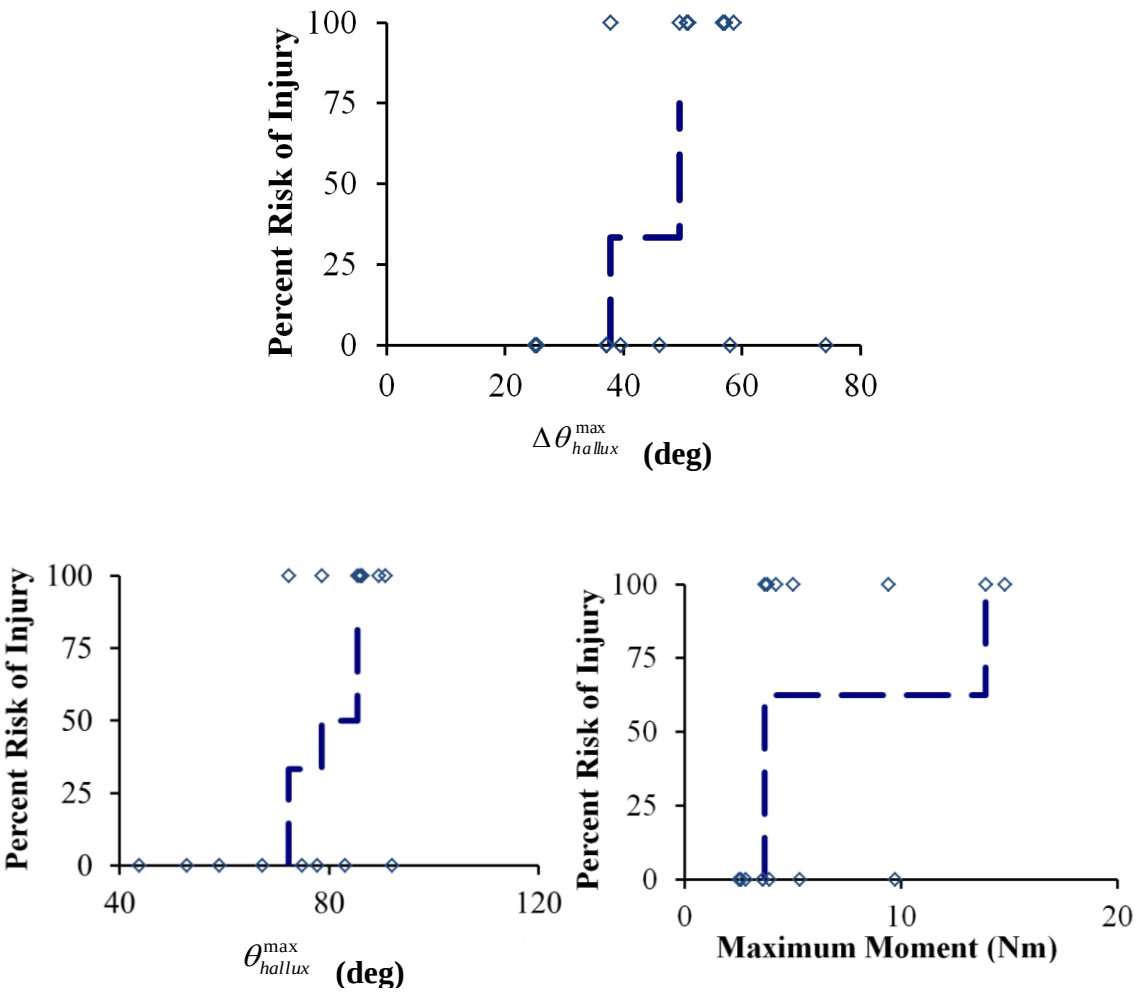

Figure 18 - non-parametric injury risk functions with overlaid tested specimens.

The parametric risk function for maximum moment from the ML method was determined to be (7):

$$P^I = 1 - e^{-(M/7.33)^{1.35}} \tag{7}$$

A 50% risk of injury was found at 6 Nm (*Figure 19*).

Minitab reported a data error during analysis for the LS estimation routine.

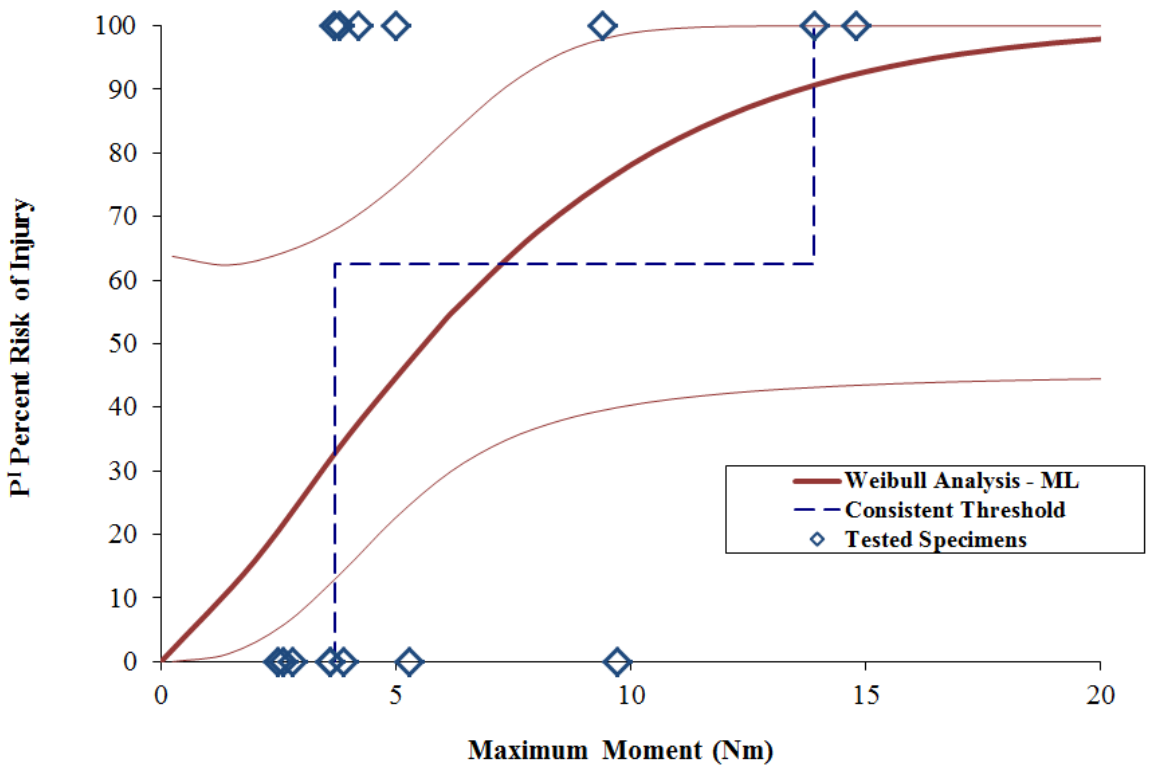

Figure 19 - injury risk function for maximum moment. The thin lines represent 95% confidence intervals.

The risk function for $\theta_{hallux}^{\max}$ according to the ML method was created (8):

$$P^I = 1 - e^{-(\theta_{hallux}^{\max}/85.21)^{5.9}} \quad (8)$$

When this function was fit to the data, the 50% risk of injury corresponded to an extension angle of 80° (

Figure 20).

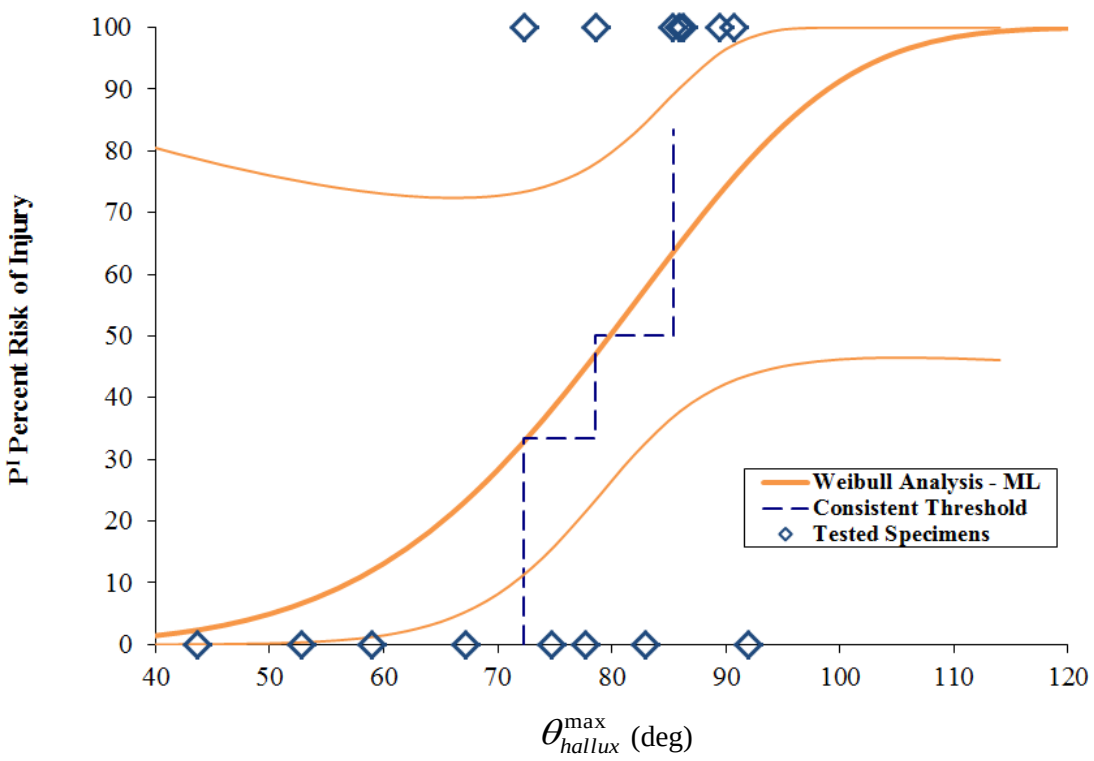

Figure 20 - injury risk function for maximum hallux angle according to the maximum likelihood algorithm (ML). The thin lines represent 95% confidence intervals.

The risk function for $\theta_{hallux}^{\max}$ according to the LS method was also created (9):

$$P^I = 1 - e^{-(\theta_{hallux}^{\max}/80.57)^{9.2}} \tag{9}$$

The LS method describes a 50% risk of injury at 78° of 1MTP extension (*Figure 21*).

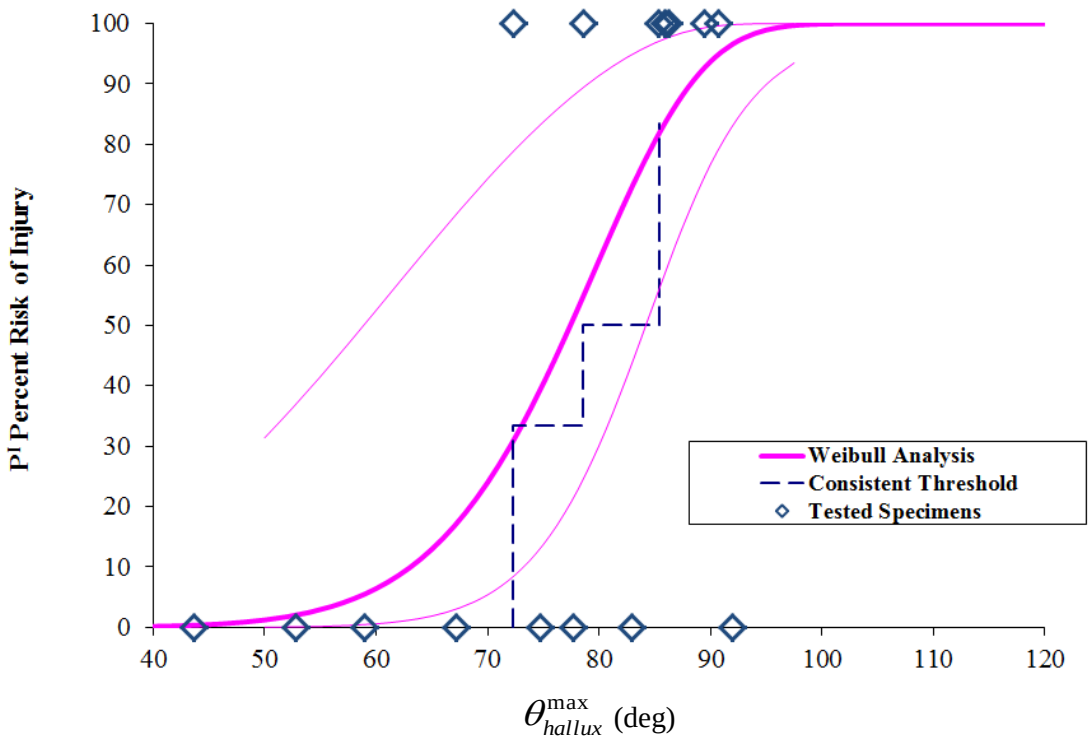

Figure 21 - injury risk functions for maximum hallux angle according to the least squares algorithm (LS). The thin lines represent 95% confidence intervals.

The risk function for $\Delta\theta_{hallux}^{\max}$ according to the ML method was created (10):

$$P^I = 1 - e^{-(\Delta\theta_{hallux}^{\max}/53.2)^{3.4}} \tag{10}$$

The ML method describes a 50% risk of injury at a change of 48° from the start of the test (*Figure 22*).

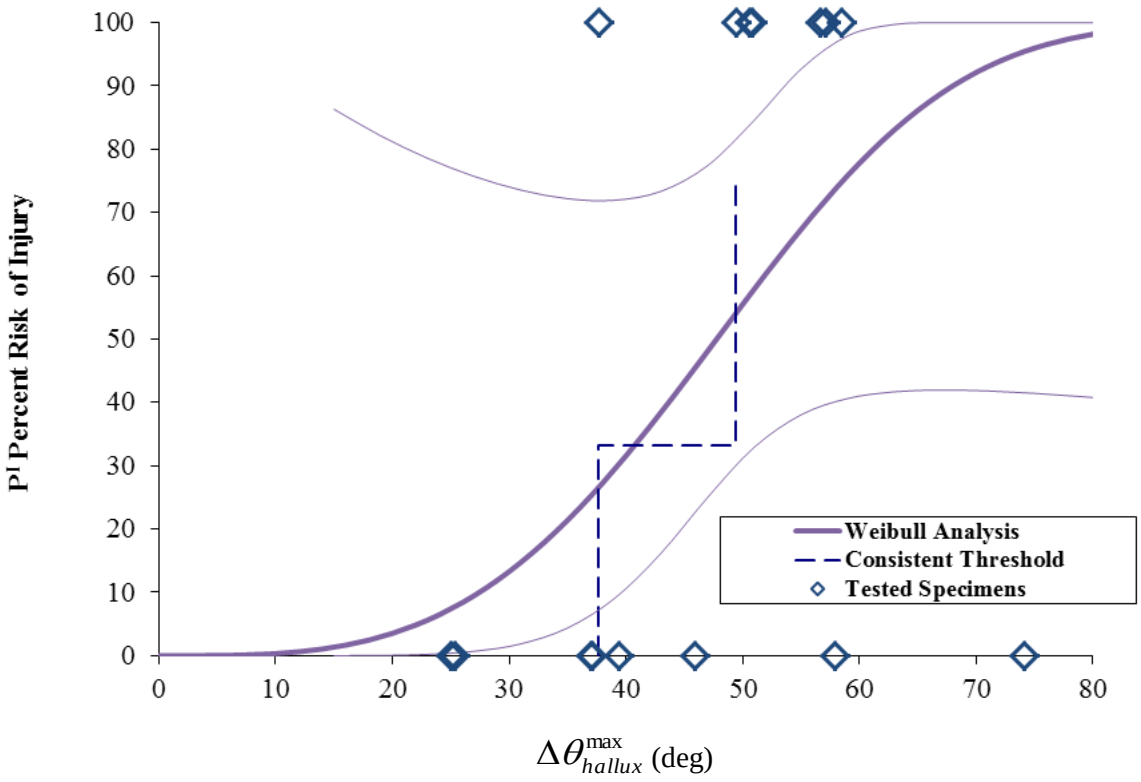

Figure 22 - injury risk function for maximum delta hallux angle according to the maximum likelihood algorithm (ML). The thin lines represent 95% confidence intervals.

The risk function for $\Delta\theta_{hallux}^{\max}$ according to the LS method was also created (11):

$$P^I = 1 - e^{-(\Delta\theta_{hallux}^{\max}/46.8)^{4.2}} \tag{11}$$

The LS method describes a 50% risk of injury at a change of 43° from the start of the test (*Figure 23*).

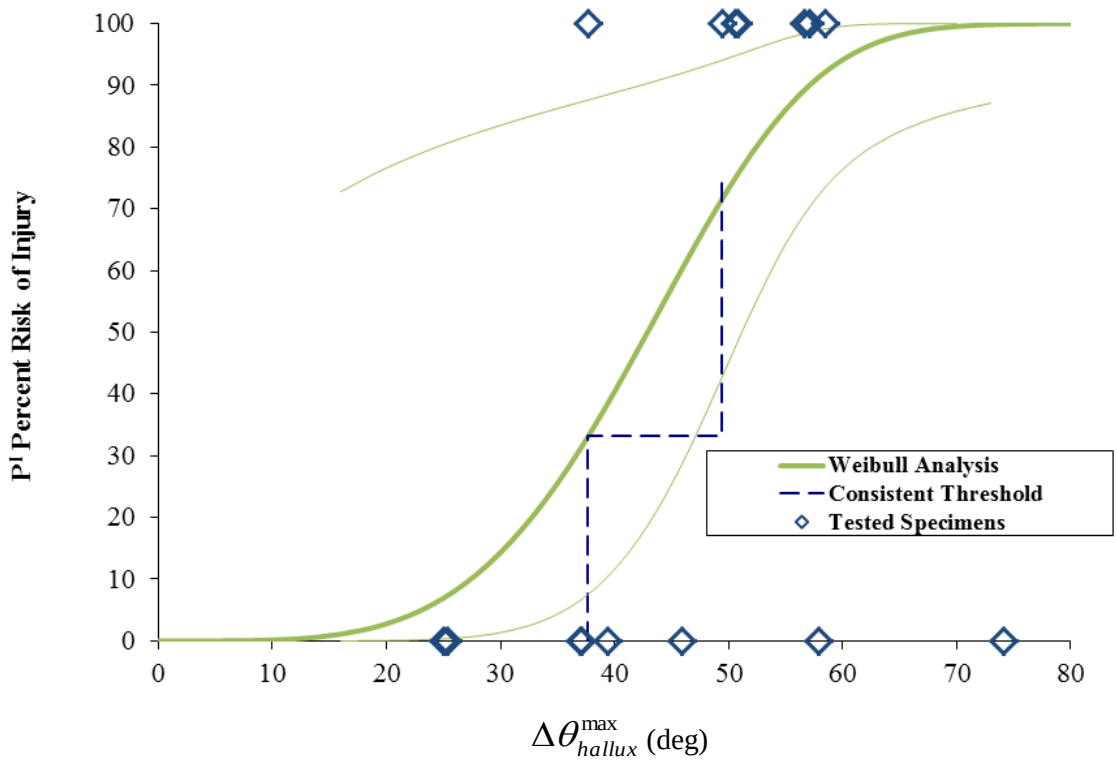

Figure 23 - injury risk function for maximum delta hallux angle according to the least squares algorithm (LS). The thin lines represent 95% confidence intervals.

3.4. Discussion

The goal of this task was to form the data gathered during cadaver testing into injury risk functions. The cadaver tests confirmed hyperextension as an injury mechanism; however, another tool was needed to interpret these data. Survival analysis formed the doubly-censored data into an easily interpretable format to assess risk based upon kinematic and kinetic parameters recorded.

Discriminative ability was reflected in the Goodman-Kruskal's Gamma and percent concordance assessment. These quantitative measures are reflected in the injury plots of each variable (*Figure 17*). To correctly predict injury/non-injury, there must be a defined transition from a range of low stimuli values, which result in non-injury, to a range of greater stimuli, which result in injury. From this, specimen number and foot aspect could have been immediately discarded from further analysis because injury occurs at a lower stimulus than non-injury results. This intuitive approach is reflected in low Gamma and concordance values. Conversely, the variables which had the best discrimination were those which exhibited a defined transition zone, with several low stimulus values to indicate non-injury before injurious specimens consistently occurred at higher stimulus levels.

Both maximum extension angle and maximum moment were found to discriminate between injurious and non-injurious conditions. However, these two variables differ considerably in their complexity and implications. Maximum extension angle was directly obtained from the motion-capture analysis. A 0° was anatomically

defined for each specimen, and maximum angle was computed from a specimen-specific model. No assumptions were made regarding starting angle, maximum angle, or specimen-specific anatomy. Conversely, maximum moment was computed using the pressure mat, load cell, and motion-capture data. To calculate the moment arm length, an assumption was made regarding hallux anatomy. Tension through the FHL, as well as post-mortem effects, induced flexion in the joint between the distal and plantar phalanx; the moment arm calculations assumed a straight-line distance between the center of pressure on the pressure mat and the 1MTP center of rotation. Compliance in the distal-plantar phalanx joint was not taken into account during moment arm calculation. Furthermore, because the test fixture oscillated during deceleration, the load cell data trace recorded "ringing" as an inertial artifact. As a result, the load used to calculate maximum moment did not coincide with the maximum test fixture rotation. Though statistics show that both maximum extension angle and maximum moment were good predictors of injury, the engineering assumptions needed to manipulate maximum moment render maximum hyperextension as the more rigorous predictor of injury.

Additionally, hyperextension angle is a valuable variable due to the non-dimensional nature of angle-to-failure (i.e. arc length/radius = length/length). The difference between tested and target populations is of concern to any test series. In injury biomechanics, it is often necessary to scale the testing results to a non-represented population. Kinetic parameters (e.g. moment) must be scaled based upon both geometric and material properties. However, because angle is a kinematic, non-dimensional variable, it is not necessary to scale an angle-to-failure injury criterion when comparing

geometrically-similar, size-different systems. Another advantage of an injury risk function based upon hyperextension angle is the lack of geometric scaling necessary between test specimens and target athletes.

The statistical software used to analyze these data was programmed with two estimation routines, and both were used to create the injury risk functions. In describing $\theta_{hallux}^{\max}$, the Weibull shape parameter nearly doubled between the ML to LS methods, while the scale parameter changed only 5%. This is reflected in the limited difference in extension angle at 50% risk of injury (2°). Both curves were close to the non-parametric form. As such, the same conclusions may be drawn from either curve. In the following chapter discussing the tradeoff between performance demands and injury risk, both curves show a separation between non-injurious and injurious maximum 1MTP extension angle.

The 1MTP angle found at 50% risk of injury (80°), is reasonable based upon previous studies for 1MTP ROM. It is important to note that the definition of 1MTP angle varies throughout literature. This thesis did not assign a 0° position to that found in the standing, neutral attitude. The anatomically based 0° position used in this work may be as much as 16° different than other studies (Buell et al. 1988). Published values of 1MTP extension ROM range between 49° and 82° (Buell et al. 1988, Eggert 1990, Joseph 1954, Nawoczenski et al. 1999, Rodeo et al. 1993, Shereff et al. 1986). Extension at 50% risk of injury is at the limit of passive ROM for all but one previously published study (Buell and Green 1988). As such, it is reasonable to expect that injury would occur around this value.

The obvious difference between tested samples and target populations, and a limitation of this study, was the use of cadaveric specimens. The tested specimens differed from the target young, athletic population in age, material properties, and environment. Literature is equivocal on how age and ultimate strain in soft tissue may be related. Many sources claim a weak, negative correlation between age and ultimate stress (Dorlot et al. 1980, Blevins et al. 1994, Noyes and Grood 1976, Woo et al. 1991, Yamada and Evans 1970). However, extension angle is a measure of ultimate strain. Flahiff et al. (1995) suggest that there is no significant relationship between age and tendon percent elongation at failure up to age 55 years. As the specimens in this study have an average age of 46.5 years at time of death, it is unlikely that age scaling would significantly alter the injury risk function.

A possible limitation of the data analysis and development of injury risk functions was the small sample size of tested specimens. 15 specimens were included in the final data set from an original sample of 21 specimens. One specimen, 416 L, was excluded because the FHL cam clamp fell of immediately prior to testing. Apart from this testing anomaly, neither the specimen condition (e.g. arthritis) nor availability of data (e.g. motion-capture failure) was compromised. When 416 L was included in the data analysis, both $\theta_{hallux}^{\max}$ and maximum moment increased to $\gamma = 0.66$, and $\Delta\theta_{hallux}^{\max}$ increased to $\gamma = 0.56$. The shape and scale parameters changed by less than 4% for $\theta_{hallux}^{\max}$ and less than 7% for maximum moment. The distribution parameters did not change for $\Delta\theta_{hallux}^{\max}$. This small change in distribution parameters suggest that though a small sample is used

for data analysis, the resulting injury risk functions for $\theta_{hallux}^{\max}$ are insensitive to the inclusion of specimen 416 L in the data analysis.

Testing environment (i.e. temperature) was a possible limitation to the interpretation of the injury risk functions. All of the PMHS tests were conducted at room temperature, approximately 28 °F cooler than body temperature. However, while ultimate stress and stiffness have been found to be temperature dependent, ultimate strain has not been shown to be temperature dependent (Bass et al. 2007, Haut and Powlison 1990, Woo et al. 1987). Because of this, the injury risk function for $\theta_{hallux}^{\max}$ was unlikely to change based upon testing temperature.

Another possible confounding variable in the analysis of these tested specimens was longitudinal arch height. A high-arched foot will have a greater $\theta_{hallux}^{t=0}$ than a low-arched foot. Because extension angle can be thought of as a synonym for strain in this analysis, the high-arched foot will be closer to the ultimate strain of the plantar plate at the start of the test than the low-arched foot, and, subsequently, the 1MTP extension angle at plantar plate failure will be lower for the high-arched foot. Thus, a high-arched foot may be predisposed to lower $\theta_{hallux}^{\max}$ before failure. As such, the high-arched foot will incur a lower $\Delta\theta_{hallux}^{\max}$ relative to a low-arched foot in order to reach an equivalent $\theta_{hallux}^{\max}$. However, this implication was not of great concern because $\theta_{hallux}^{\max}$ was found to be more predictive of injury than $\Delta\theta_{hallux}^{\max}$. Also, it follows that $\theta_{hallux}^{t=0}$ was a poor predictor of injury. This variable, which loosely describes arch height, would be expected to be a good predictor of injury if arch height, or $\Delta\theta_{hallux}^{\max}$, discriminated injury outcome. At the

same time, it should be noted that arch height is influenced by muscle activation as well as ground reaction force (e.g. Headlee et al. 2008). The influence of arch height to 1MTP sprain in an athlete may not be fully described by a cadaver-based injury risk function.

Though chronic injury and mild sprain were not the focus of this study, two specimens, 486 L and 487 R, were noted during necropsy with possible attenuation or laxity in the plantar plate but without noticeable tears. The inclusion of these specimens did not change the injury risk function for $\theta_{hallux}^{\max}$, though γ rose to 0.63. With the addition of the two specimens as injurious, $\Delta\theta_{hallux}^{\max}$ became more discriminating (γ = 0.63), and the risk functions for this parameter changed to a scale parameter of 46.4 and scale parameter of 3.3 for the ML method and scale parameter of 36.1 and shape parameter of 2.1 for the LS method. Maximum moment rose to a γ = 0.93; Minitab reported a data error for the LS method, but the ML method changed to a shape parameter of 15.6 and a scale parameter of 3.9. By including 486 L and 487 R as injurious, the injury criteria reflected a more relaxed injury definition in which sprain was defined before the onset of ligament tear. However, simply including these two specimens as injured does not fully describe a less severe injury threshold. The necropsy did not specifically examine for attenuation, and other specimens may not have been classified as attenuated due to the subjective nature of this diagnosis. Furthermore, guidelines for identifying attenuation were not defined and the physicians performing the necropsy were not directed in their classification of attenuation versus integrity of the ligament. The changes in parameters when including these two specimens suggest that injury threshold depends upon injury definition, yet due to the limitation on diagnosing attenuation, these parameters should

not be used to define a threshold of mild 1MTP sprain. Future work should develop data and injury risk functions for less severe and chronic 1MTP sprain.

This interpretation of the cadaver test data provided a geometrically-consistent variable shown to discriminate between injurious and non-injurious tests: maximum hallux extension. Through survival analysis methods, the data from the cadaver test series were formed into a continuous injury risk function based upon a Weibull distribution. It is reasonable to expect that a 50% risk of injury occurs at 80° of 1MTP extension.

4. Evaluation of Performance-Risk Tradeoff and Application to Shoe Design

An obvious application of the injury risk curve developed in the previous chapter is the design of shoes to mitigate the risk of 1MTP sprain. This application requires, of course, consideration of factors other than risk mitigation, including the athlete's performance while wearing the shoe. While a full exploration of the performance-risk tradeoff in shoe design is outside the scope of this thesis work, consideration of athlete performance data provides valuable context for the interpretation and use of the cadaver-based injury risk function reported here.

The previous chapters have detailed the creation of 1MTP sprain and the development of injury criteria from these tests. The background for this test series also introduced a performance study describing joint motion during non-injurious athletic situations. In order to begin evaluating the performance-risk tradeoff, these two metrics, performance and injurious kinematics, must be in equivalent form. The most convenient way to do so is to fit the performance data to a parametric cumulative density function (CDF). Instead of describing injury risk like the CDFs developed in the previous chapter, the performance CDF describes the likelihood of an athlete attaining a degree of 1MTP extension. With both injury risk and performance likelihood modeled as Weibull distributions, comparison between the two is possible.

The main obstacle to immediately fitting the two curves on the same plot is the difference in motion-capture methodology used to obtain each curve. The cadaver test

series measured joint kinematics through marker arrays rigidly attached to bone. Clearly this methodology is inappropriate for use on living athletes. During the performance study, motion-capture markers were attached with adhesive to the skin of athletes and the resulting motion was analyzed using a simplified foot model. Artifacts of skin and subcutaneous soft tissue are not removed from this motion analysis.

This chapter develops a regression function from the skin-based description of 1MTP extension to that of the bone-based cadaver studies. Subsequently, this chapter describes the interaction between these two methods and interprets the results.

4.1. Motion-Capture Method Alignment

The objective of this study was to quantify the difference in bone-based and skin-based 1MTP extension and to generate a function relating skin-based extension angle (θ_{SB}) to bone-based extension angle (θ_{BB}) so that cadaver-based injury data and in vivo performance data may be compared.

4.1.1. Methods

Lower-limbs were transected mid tibia-fibula from PMHS specimens. All testing was conducted with approval from the University of Virginia (UVA) Center for Applied Biomechanics Oversight Committee and the UVA Institutional Biosafety Committee. Non-reflective, self-adherent material (3M; St. Paul, MN) was used to cover each specimen. Rigid arrays were placed according to the protocol for the test series described in the previous chapter. Pre-test CTs again confirmed array placement and absence of injury. Immediately prior to testing, skin-based markers were placed according to the

protocol used for the athlete performance study (described in Chapter 2.1.1). During testing, these two marker sets were evaluated simultaneously (*Figure 24*).

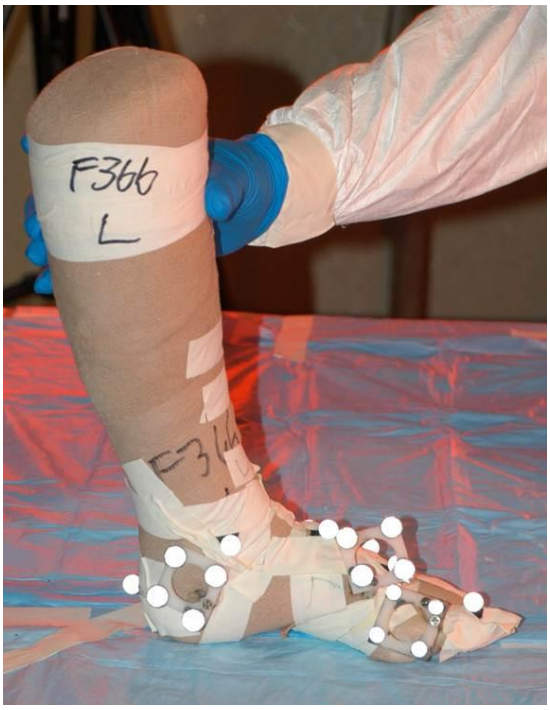

Figure 24 - PMHS specimen used in manipulation study immediately prior to testing. Both rigid arrays and skin-adhered markers are shown on the specimen.

Each specimen was manually manipulated through a continuous series of gait cycle events: foot-flat, heel-off, fore-foot eversion and inversion, and toe-off. Manipulation was performed on a hard, level surface within the calibrated viewing volume of eight Vicon MX13 cameras (Vicon Motion Systems; Oxford, UK) recording at 1,000 Hz.

Rigid-marker analysis was conducted as previously described (see Chapter 2.2). OpenSim model foot segments were scaled using measurements from CT, and inverse

kinematics in this same program were used to calculate θ_{SB}. The model comprised of three rigid bodies representing 1.) hind-foot (three markers; calcaneus and tarsal bones), 2.) fore-foot (two markers; metatarsals), and 3.) phalanges (one marker) (*Figure 25*). A ball joint, defined common to both the hind-foot and fore-foot segments, provided a rotation-only link between the two. A mediolateral revolute joint was imposed at the 1MTP joint. Sagittal plane motion, θ_{SB}, was described about this joint. Two coordinate systems were imposed to determine a zero-angle position of the foot (*Figure 25*). The alignment of the two x-axes defined the zero-angle.

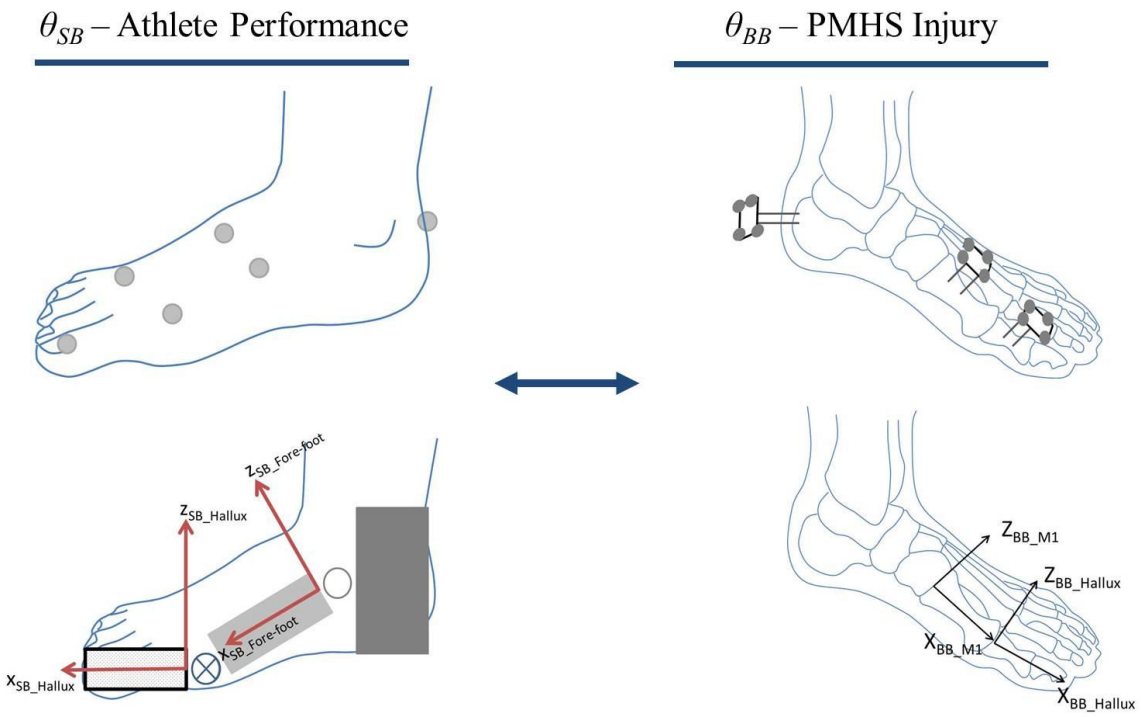

Figure 25 - schematic of skin and bone marker sets and respective models for analysis. The skin marker set is grouped into three rigid bodies, and a hinge-only joint is modeled between the fore-foot and hallux. The bone marker arrays are rigidly attached and directly provide 6DoF motion.

Table 8 - coordinate systems used in analysis of each motion-capture methodology.

Model	Coordinate System	X-Axis	Y-Axis	Z-Axis
θ_{BB}	M1	Center of base to center of head	Parallel to line connecting most plantar point of sesamoids	Orthogonal
	Hallux	Center of PP1 base to center of PP1 head	Parallel to plantar surface of distal head	Orthogonal
θ_{SB}	Fore-foot	From ball joint to center of proximal end of met1 segment	Mediolateral	Orthogonal
	Hallux	Center of PP1 base to center of PP1 head	Mediolaterael	Orthogonal

The manipulation resulting in the largest degree of 1MTP extension was used for all analyses. The two measured angles were cross-plotted for each specimen. Linear regression was used to define a relationship between the two measurements; R^2 values were calculated to assess fit (Excel, Microsoft Corp; Redmond, WA, USA).

4.1.2. Results

Six limbs from three female cadavers were tested. Specimen F71 – Left was excluded from final analysis due to limited visibility of motion-capture markers during testing. For all specimens, the heel-off event was found to produce the greatest 1MTP extension.

Individual specimen fits of θ_{SB} versus θ_{BB} exhibited good fit with a linear regression (R2: 0.98 – 0.99) (*Figure 26*). The slope varied from 0.51 to 0.77. Intercept values varied from -2.07 to 11.57. The slope of F72 – Right was noted as a potential outlier, and the regression function was analyzed twice: first including F72 – Right (All,

n=5), and second without F72 – Right (Subset, n=4). The relationship for the All group ($p<0.001$ for slope and offset, $R^2 = 0.90$) is given as (*Figure 26*):

$$\theta_{BB\_All} = 0.72 * \theta_{SB\_All} + 3.28 \quad (12)$$

The relationship for the subset group ($p<0.001$ for slope and offset, $R^2 = 0.95$) was found to be:

$$\theta_{BB\_Subset} = 0.75 * \theta_{SB\_Subset} + 3.58 \quad (13)$$

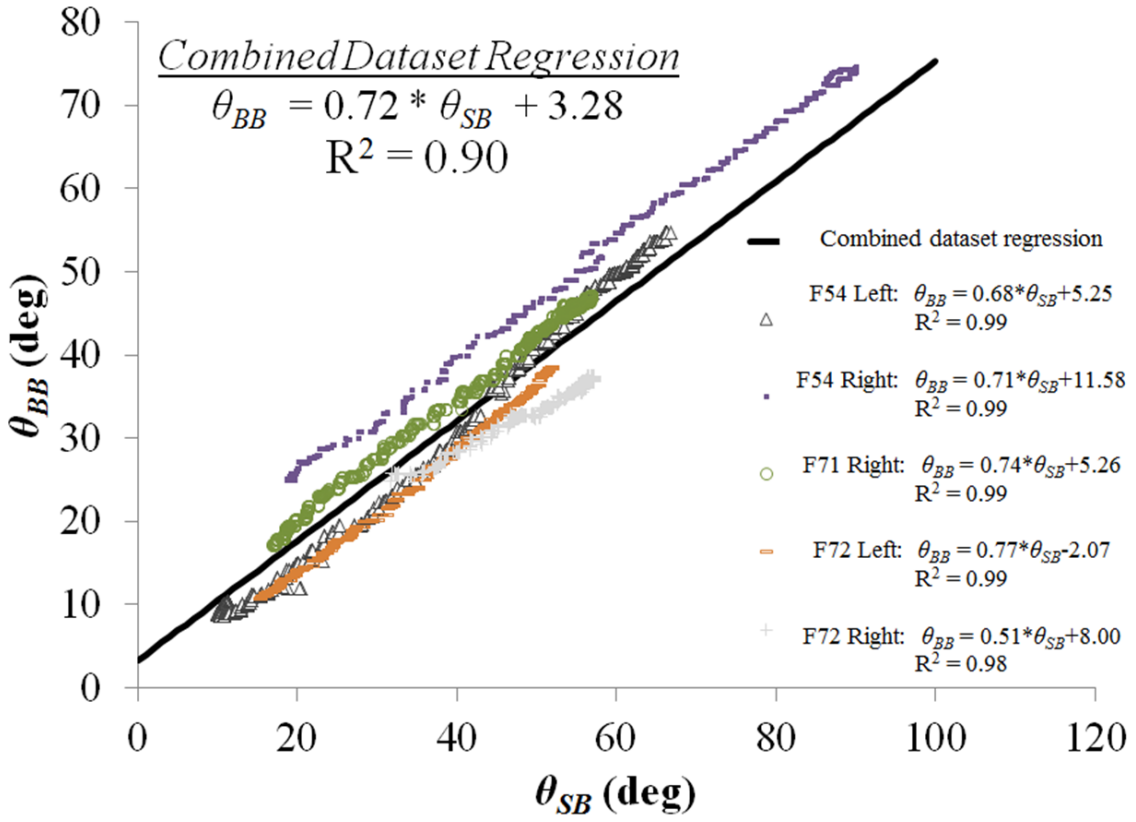

Figure 26 - data and linear regression for each of the five tested and analyzed specimens. Regression for the All dataset is also given.

4.1.3. Discussion

This study developed a methodology and a data set to describe the relationship between θ_{SB}, used to describe motion of living subjects, and θ_{BB}, used to describe motion in cadaveric test specimens. This relationship was needed to convert between the two methods because, as shown, θ_{SB} was not equal to θ_{BB}.

Though the same researcher performed the manipulation on all specimens, exact kinematics were not prescribed, and inter-specimen variations in motion were allowed. This variation was advantageous because the relationship developed here must hold for large variations in gait. This study was designed to relate two kinematic descriptions of 1MTP extension to each other, with the goal of applying this relationship to performance kinematics of athletes. Thus, achieving an experimental ROM comparable to performance ROM was required, rather than standardizing exact motions. The maximum θ_{SB} found in this study ranged from 52 – 89°, which was within the range of previously published maximum 1MTP extension angles for elite athletes (Riley et al., 2012). As such, the experimental methods used to establish the θ_{SB}- θ_{BB} relationship was appropriate to *in vivo* 1MTP joint motion.

Visual inspection of the datasets led the authors to develop two groups, and two regressions, for the test data analysis. Though no technical difficulty (e.g. view limitation on motion-capture) was noted for the exclusion of F72 – Right, the limited motion induced in this specimen (θ_{BB}: 25 – 37°) was thought to have skewed the regression equation. The resultant regression for the Subset group exhibited a slightly better fit for the data than the All group, as exhibited by R^2 values. A larger dataset is needed to

determine if this specimen is truly an outlier. Further study with greater variation in specimen characteristics (e.g. gender, age, mass) would help clarify the sensitivity of the relationship. Until this uncertainty is clarified, the All regression should be used.

4.2. Revision of Performance Evaluation

Using the All group regression equation developed above, the maximum 1MTP extension angle from walking, running, cutting, or starting for each player recorded during the athlete performance study (Riley et al. 2012) was revised to reflect extension in θ_{BB} (*Figure 27*). The difference between θ_{SB} and θ_{SB} of the performance data was statistically significant ($p<<0.01$) as assessed by a two-parameter t-test. In the original skin reference system, 50% likelihood of maximum 1MTP extension attained by athletes was 86°. Transformed to the bone reference system, this 50% likelihood attained by athletes was 52°.

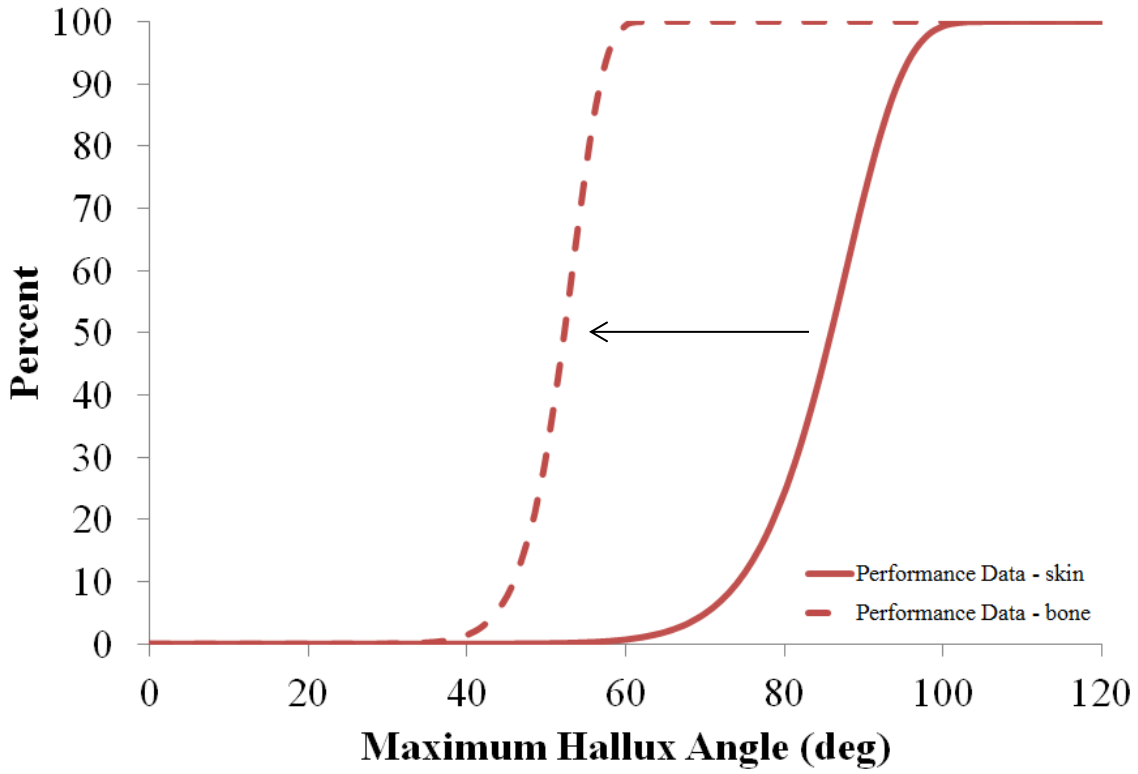

Figure 27 - revision of athlete performance data from motion-capture alignment study.

4.3. Interpretation

The manipulation study was necessary to reconcile the performance and injury motion-capture methods. After the performance data was transformed to the bone reference system, both evaluations were plotted in the same space (*Figure 28*).

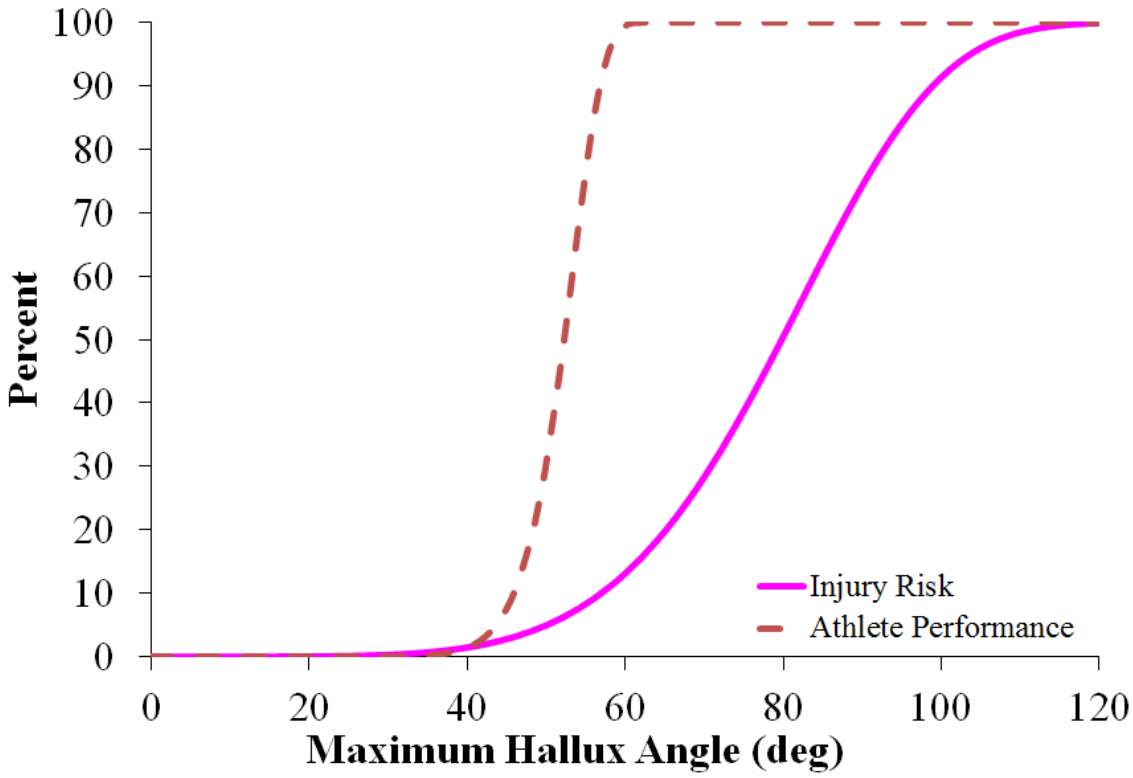

Figure 28 - performance and injury plotted in the same space. The gap between the two curves represents a design opportunity for equipment manufacturers.

This plot showed the space between what athletes desire for performance and the threshold of 1MTP sprain according to $\theta_{hallux}^{\max}$. One method of analyzing this space was to look at the distance between the angles of extension at 50% likelihood. The athlete performance reached 50% likelihood at 52° of 1MTP extension while the injury risk function reached 50% chance of sprain at 86° of 1MTP extension. The 34° difference between the two measures indicated that 1MTP extension typically used for athletic performance ends before injurious extension begins. A second method of interpreting the data was to look at the disparity in likelihood for a given 1MTP angle. For example, 99.9% of players never exceeded 64° of 1MTP extension during non-injurious motion.

At this same angle, there was only an 18% chance of injury. By reconciling the motion-capture methods used to record performance data and to analyze injury risk, this task has shown the gap between 1MTP extension needed for performance and joint extension at onset of acute injury.

The performance-risk tradeoff and the resulting design space were the result of comparing a cadaver-based injury criterion with a description of performance from living, elite athletes. It is out of the scope of this thesis to translate the cadaver-based injury criterion to an injury criterion based upon living athletes. However, it is important to be aware of the limitations of this comparison. For example, the cadaver injury model did not include any muscle tension proximal to the sesamoids. It may be that when intrinsic foot muscles such as the FHB are active, the motion of the sesamoids are limited earlier in hallux extension, resulting in increased strain in the plantar plate. This in turn may result in injury at a lower extension, thus shifting the injury criterion curve to the left. Though this work begins to describe the interaction between athlete performance and injury, future work should endeavor to describe the space between two curves both based upon living, elite athletes.

5. Conclusions and Contributions

The work of this thesis created an injury risk function for 1MTP sprain in hyperextension and evaluated the performance-risk tradeoff using previously obtained performance data. Initially this work used kinematic information obtained from athlete performance trials to inform test fixture design of 1MTP hyperextension. This fixture was then used to test PMHS specimens in hyperextension at both injurious and sub-injurious levels. The kinematic and kinetic engineering parameters acquired from testing were then assessed for discrimination. Extension angle was determined to be the most useful variable both for its predictive ability and because of the utility of a non-dimensional property in eliminating the necessity of geometric scaling. Motion-capture methods were aligned through a manipulation study so that performance and injury angle were comparable. When transformed into the same reference and plotted together, a significant difference between performance requirements and the injurious regime was described.

This work was the first to conclusively establish hyperextension as an injury mechanism for 1MTP sprains. Though many retrospective accounts had been published suggesting this injury mechanism, this was the first work to demonstrate repeatable, clinically-representative injury through this mechanism. The injury created was judged to be representative of what is seen in the field by medical professionals experienced with this trauma. Sub-injurious trials also confirmed hyperextension as an injury mechanism. By varying the amount of rotation to induce or prevent injury, these tests demonstrate the certainty of hyperextension as an injury mechanism for 1MTP sprain.

The final step in the work discussed here was to link the hyperextension injury data to 1MTP extension records of athletes. Performance and prevention must be balanced when mitigating the risk of 1MTP sprain in athletes. Contemporary attempts to prevent 1MTP sprain typically take the form of foot orthoses or extended steel shanks placed in the sole of a hoe to limit hallux extension (Nawoczenski and Janisse 2004). However, because these devices are not designed with performance-injury tradeoff data, they aggressively limit 1MTP ROM to such an extent that athlete performance is compromised. As a result, the orthoses or steel shanks are used post-injury rather than as a preventative measure. Effective injury prevention must be designed to allow maximum movement before limiting ROM close to injury threshold. The combination of performance kinematics and injury risk defines this threshold.

This performance-injury risk information has been provided to shoe manufacturers (Nike and Under Armour) as well as the National Football League. The design space created between the performance likelihood curve and the injury risk function will help to guide design of future shoe models.

While this work makes great strides to improve shoe and orthoses design parameters, it is still limited by the use of PMHS specimens. Future work should investigate the effects of muscle activation as well as non-proportional scaling to the injury risk function. The sesamoids are ossified sections of the FHB. As such, their movement during extension may be limited based upon FHB activation. 1MTP sprain occurs distal to the sesamoids, and restricted sesamoid motion may lower the threshold of injury resulting from increased strain in this region. Similarly, future work should

determine the difference and effect of an athlete's tendon, ligament, and muscle cross-sectional area as compared to that of PMHS specimens. For example, mechanical loading stimulates remodeling in orthopedic tissues; therefore, athletes who experience large loads repeatedly on their lower limbs may have greater plantar plate thickness than a non-athlete. Though strain is non-dimensional, this difference in thickness may alter the angle at which injury occurs when muscles forces are integrated to the injury model.

This thesis establishes a new standard for designing protective equipment to prevent 1MTP joint sprains. The interaction of athlete performance and injury risk were used to establish an appropriate equipment design space. With this information, it is my hope that both the frequency and severity of turf toe injuries are significantly lower in the near future.

6. References

[Allen et al. 2004] Allen LR, Flemming D, Sanders TG. Turf toe: ligamentous injury of the first metatarsophalangeal joint. Mil Med. 2004;169(11):xix-xxiv.

[Badekas et al. 2009] Badekas T, Papadakis SA, Vergados N, et al. Foot and ankle injuries during the Athens 2004 Olympic Games. J Foot Ankle Res. 2009;2(1):9.

[Bass et al. 2007] Bass CR, Planchak CJ, Salzar RS, Lucas SR, Rafaels KA, Shender BS, Paskoff G. The temperature-dependent viscoelasticity of porcine lumbar spine ligaments. SPINE. 2007;32(16):E436-E442.

[Blevins et al. 1994] Blevins FT, Hecker AT, Bigler GT, Boland AL, Hayes WC. The effects of donor age and strain rate on the biomechanical properties of bone-patellar tendon-bone allografts. Am. J. Sports Med. 1994;22(3):328-333.

[Bowers and Martin 1976] Bowers KD Jr, Martin RB. Turf-toe: a shoe-surface related football injury. Med Sci Sports. 1976;8(2):81-83.

[Brophy et al. 2009] Brophy RH, Gamradt SC, Ellis SJ, et al. Effect of turf toe on foot contact pressures in professional American football players. Foot Ankle Int. 2009;30(5):405-409.

[Buell et al. 1988] Buell T, Green DR, Risser J. Measurement of the first metatarsophalangeal joint range of motion. J Am Podiatr Assoc. 1988;78(9):439-448.

[Clanton et al. 1986] Clanton TO, Butler JE, Eggert A. Injuries to the metatarsophalangeal joints in athletes. Foot Ankle. 1986;7(3):162-176.

[Coker et al. 1978] Coker TP, Arnold JA, Weber DL. Traumatic lesions of the metatarsophalangeal joint of the great toe in athletes. Am J Sports Med. 1978;6(6):326-334.

[DiDomenico and Nusholtz 2003] DiDomenico L, Nusholtz G. Compairison of parametric and non-parametric methods for determining injury risk. SAE Technical Paper 2003-01-1362, 2003.

[Dorlot et al. 1980] Dorlot JM, Sidi MAB, Tremblay GM, Brouin G. Load elongation behavior of the canine anterior cruciate ligament. J. Biomech. Engr. 1980;102:190-193.

[Eggert 1990] Eggert KE. First Metatarsophalangeal Joint Range of Motion as a Factor in Turf Toe Injuries. Master's Thesis. 1990. Univeristy of Houston, Houston, TX.

[Fabeck et al. 2002] Fabeck LG, Zekhnini C, Farrokh D, Descamps P-Y, Delincé PE. Traumatic hallux valgus following rupture of the medial collateral ligament of the first metatarsophalangeal joint: a case report. J Foot Ankle Surg. 2002;41(2):125-128.

[Flahiff et al. 1995] Flahiff CM, Brooks AT, Hollis JM, Vander Schilden JL, Nicholas RW. Biomechanical analysis of patellar tendon allografts as a function of donor age. Am. Orth. Soc. Sports Med. 1995;23(3):354-358.

[Frimenko et al. 2012] Frimenko RE, Lievers WB, Coughlin MJ, Anderson RB, Crandall JR, Kent RW. Etiology and biomechanics of first metatarsophalangeal joint sprains (turf toe) in athletes. Crit. Reviews Bio. Engr. 2012;40(1):43-61.

[Ford et al. 2006] Ford KR, Manson NA, Evans BJ, Myer GD, Gwin RC, Heidt RS Jr, Hewett TE. Comparison of in-shoe foot loading patterns on natural grass and synthetic turf. J Sci Med Sport. 2006;9:433-440.

[Funk 2000] Funk JR. The Effect of Active Muscle Tension on the Axial Impact Tolerance of the Human Foot/Ankle Complex. Doctoral Dissertation. 2000. University of Virginia, Charlottesville, VA.

[Funk et al. 2002] Funk JR, Rudd RW, Srinivasan SCM, King RJ, Crandall JR, Petit PY. Methodology for measuring tibial and fibular loads in a cadaver. SAE Technical Paper. 2002-01-0682.

[Genschel and Meeker 2010] Genschel U, Meeker WQ. A comparison of maximum likelihood and median-rank regression for Weibull estimation. Quality Engr. 2010;22:236-255.

[Graves et al. 1991] Graves SC, Prieskorn D, MannRA. Posttraumatic proximal migration of the first metatarsophalangeal joint sesamoids: a report of four cases. Foot Ankle. 1991;12(2):117-122.

[Haut and Powlison 1990] Haut RC, Powlison AC. The effects of test environment and cyclic stretching on the failure properties of human patellar tendon. J. Ortho. Research. 1990;8:532-540.

[Headlee et al. 2008] Headlee DL, Leonard JL, Hart JM, Ingersoll CD, Hertel J. Fatigue of the plantar intrinsic foot muscles increases navicular drop. J. Electromyography and Kinesiology. 2008;18:420-425.

[Hetherington et al. 1992] Hetherington VJ, Chessman GW, Steuben C. Forces on the first metatarsophalangeal joint: a pilot study. J Foot Surg. 1992;31(5):450-453.

[Hicks 1954] Hicks JH. The mechanics of the foot, II: the plantar aponeurosis and the arch. J Anat. 1954;88(pt 1):25-30.

[Hosmer and Lemeshow 1999] Hosmer DW, Lemeshow S. Applied Survival Analysis: Regression Modeling of Time to Event Data. John Wiley & Sons Inc. New York, NY: 1999.

[Joseph 1954] Joseph J. Range of movement of the great toe in men. J Bone Joint Surg. 1954;36B(3):450-457.

[Kaplan et al. 2011] Kaplan LD, Jost PW, Honkamp N, Norwig J, West R, Bradley JP. Incidence and variance of foot and ankle injuries in elite college football players. Am J Ortho. 2011;40(1):40-44.

[Karadaglis and Grace 2003] Karadaglis D, Grace D. Morphology of the hallux sesamoids. Foot Ankle Surg. 2003;9(3):165-167.

[Kent and Funk 2004] Kent RW, Funk JR. Data censoring and parametric distribution assignment in the development of injury risk functions from biomechanical data. SAE Tech. Paper 2001-01-0317:2004.

[Kent et al. 2008] Kent RW, Stacey S, Kindig M, Woods W, Evans J, Rouhana SW, Higuchi K, Tanji H, St. Lawrence S, Arbogast KB. Biomechanical response of the pediatric abdomen, part 2: injuries and their correlation with engineering parameters. Stapp Car Crash J. 2008;52:1-32.

[Kubitz 2003] Kubitz ER. Athletic injuries of the first metatarsophalangeal joint. J Am Podiatr Med Assoc. 2003;93(4):325-332.

[Manning and Levy 2006] Manning MR, Levy RS. Soccer. Phys Med Rehab Clin North Am. 2006;17(3):677-695.

[McCormick and Anderson] McCormick JJ, Anderson RB. The great toe: failed turf toe, chronic turf toe, and complicated sesamoid injuries. Foot Ankle Clin North Am. 2009;14(2):135-150.

[Meyer et al. 1994] Meyer SA, Callaghan JJ, Albright JP, Crowley ET, Powell JW. Midfoot sprains in collegiate football players. Am J Sports Med. 1994;22(3):392-401.

[Mullis and Miller 1980] Mullis DL, Miller WE. A disabling sports injury of the great toe. Foot Ankle. 1980;1(1):22-25.

[Nawoczenski et al. 1999] Nawoczenski DA, Baumhauer JF, Umberger BR. Relationship between clinical measurements and motion of the first metatarsophalangeal joint during gait. J Bone Joint Surg. 1999;81B(3):370-376.

[Nawoczenski and Janisse 2004] Nawoczenski DA, Janisse DJ. Foot orthoses in rehabilitation – what's new. Clin Sports Med. 2004;23(1):157-167.

[Nevin 1997] Nevin C. Kinematics of the first metatarsophalangeal joint in intact and surgically altered cadavers. Foot Ankle Int. 1997;18(3):132-137.

[Noyes et al. 1974] Noyes RF, DeLucas JL, Torvik PJ. Biomechanics of anterior cruciate ligament failure: an analysis of strain-rate sensitivity and mechanisms of failure in primates. J Bone Joint Surg. 1974;56A(2):236-253.

[Noyes and Grood 1976] Noyes FR, Grood ES. The strength of the anterior cruciate ligament in humans and Rehsus monkeys. J Bone Joint Surg. 1976;58A(8):1074-1082.

[Nusholtz and Mosier 1999] Nusholtz G, Mosier R. Consisten threshold estimate for doubly censored biomechanical data. SAE Tech. Paper 1999-01-0714, 1999.

[Orendurff et al. 2008] Orendurff MS, Rohr ES, Segal AD, Medley JW, Green JR III, Kadel NJ. Regional foot pressure during running, cutting, jumping, and landing. Am J Sports Med. 2008;36(3):566-571.

[Prieskorn et al. 1995] Prieskorn D, Graves S, Yen M, Ray J Jr, Schultz R. Integrity of the first metatarsophalangeal joint: a biomechanical analysis. Foot Ankle Int. 1995;16(6):357-362.

[Richardson 1987] Richardson EG. Injuries to the hallucal sesamoids in the athlete. Foot Ankle Int. 1987;7(4):229-244.

[Riley et al. 2012] Riley P, Kent RW, Dierks TA, Lievers WB, Frimenko RE. Foot and ankle motion of professional athletes in American football-specific tasks. Gait and Posture. 2012;online 15 May 2012:doi 10.1016/j.gaitpost.2012.03.034.

[Rodeo et al. 1993] Rodeo SA, Warren RF, O'Brien SJ, Pavlov H, Barnes R, Hanks GA. Diastasis of bipartite sesamoids of the first metatarsophalangeal joint. Foot Ankle. 1993;14(8):425-434.

[Sarrafian 1993] Sarrafian SK. Anatomy of the Foot and Ankle: Descriptive, Topographic, Functional. 2nd ed. Philadelphia: J. B. Lippincott Company; 1993.

[Seireg and Arvikar 1989] Seireg A, Arvikar R. Biomechanical Analysis of the Musculoskeletal Structure for Medicine and Sports. New York, NY: Hemisphere Publishing; 1989.

[Shaw et al. 2009] Shaw G, Parent D, Purtsezov S, Lessley D, Crandall J, Kent R, Guillemot H, Ridella SA, Takhounts E, Martin P. Impact response of restrained PMHS in frontal sled tests: skeletal deformation patterns under seat belt loading. Stapp Car Crash J. 2009;53:1-48.

[Shereff et al. 1986] Shereff MJ, Bejjani FJ, Kummer FJ. Kinematics of the first metatarsophalangeal joint. J Bone Joint Surg. 1986;68A(3):392-398.

[Snow et al. 1995] Snow SW, Bohne WHO, DiCarlo E, Chang VK. Anatomy of the Achilles tendon and plantar fascia in relation to the calcaneus in various age groups. Foot & Ankle Int. 1995;16(7):418-421.

[Stokes et al. 1979] Stokes IAF, Hutton WC, Stott JRR. Forces acting on the metatarsals during normal walking. J Anat. 1979;129(pt3):579-590.

[Tewes et al. 1994] Tewes DP, Fischer DA, Fritts HM, Guanche CA. MRI findings of acute turf toe: a case report and review of anatomy. Clin Ortho Rel Res. 1994;304:200-203.

[Wilson et al. 2005] Wilson L, Dimeff R, Miniaci A, Sundaram M. First metatarsophalangeal plantar plate injury (turf toe). Orthopedics. 2005;28(4):417-419.

[Woo et al. 1987] Woo SLY, Lee TQ, Gomez MA, Sato S, Field FP. Temperature dependent behavior of the canine medial collateral ligament. Trans. Of ASME. 1987;109:68-71.

[Woo et al. 1990] Woo SLY, Peterson RH, Ohland KJ, Sites TJ, Danto MI. The effects of strain rate on the properties of the medial collateral ligament in skeletally immature and mature rabbits: a biomechanical and histological study. J. Ortho. Rsrch. 1990;8:712-721.

[Woo et al. 1991] Woo SLY, Holls M, Adams DJ, Lyon RM, Takai S. Tensile properties of the human femur-anterior cruciate ligament-tibia complex. Am. J. Sports Med. 1991;19(3):217-225.

[Yamada and Evans 1970] Yamada H, Evans FG. Strength of Biological Materials. Williams & Wilkins Co: Baltimore, MD; 1970.

7. Appendix A – PMHS Test Fixture Instrumentation

Name	CAB ID	Information
toe plate load cell	LCQ124	6-axis TNO Q-series load cell Model 3715, Serial# 124 Denton ATD, Inc.
ball of foot load cell	LCQ123	6-axis TNO Q-series load cell Model 3715, Serial# 123 Denton ATD, Inc.
heel load cell	LCGP175	6-axis load cell Model 6085, Serial# 75 Denton ATD,Inc.
tibia load cell	LCSC79	6-axis steering column load cell Model 3868, Serial# 79 Denton ATD, Inc.
FHL load cell	LC9127	Single axis load cell (50 lb) Model 31, Serial# 1109127 Honeywell
ARS 1500	ARS0152	angular rate sensor (1500 deg/s) DTS ARS, Serial# 0119 Diversified Technical Systems (DTS), Inc.
ARS 12000	ARS0119	angular rate sensor (12000 deg/s) DTS ARS, Serial# 0119 Diversified Technical Systems (DTS), Inc.
linear accelerometer	AC2830	Accelerometer (2000g) 7264B-2000, Serial# B52830 Endevco Corp.
top accelerometer	AC4236	accelerometer (2000g) Endevco 7264B-2000, Serial# B44236 Endevco Corp.
side accelerometer	AC2834	accelerometer (2000g) Endevco 7264B-2000, Serial# B52834 Endevco Corp.
string pot	DS81	Model JX-PA-80-N11-S1S-114 Serial# 34020081 UniMeasure
linear magnetic displacement transducer	DSLN	Model TLM 0950 001 413 203 Serial# 087146/09160005 Novotechnik
pressure mat	N/A	Model 3200 – Hoof F-Scan Cuff TekScan, Inc.

8. Appendix B – Data Traces

Specimen #400 R

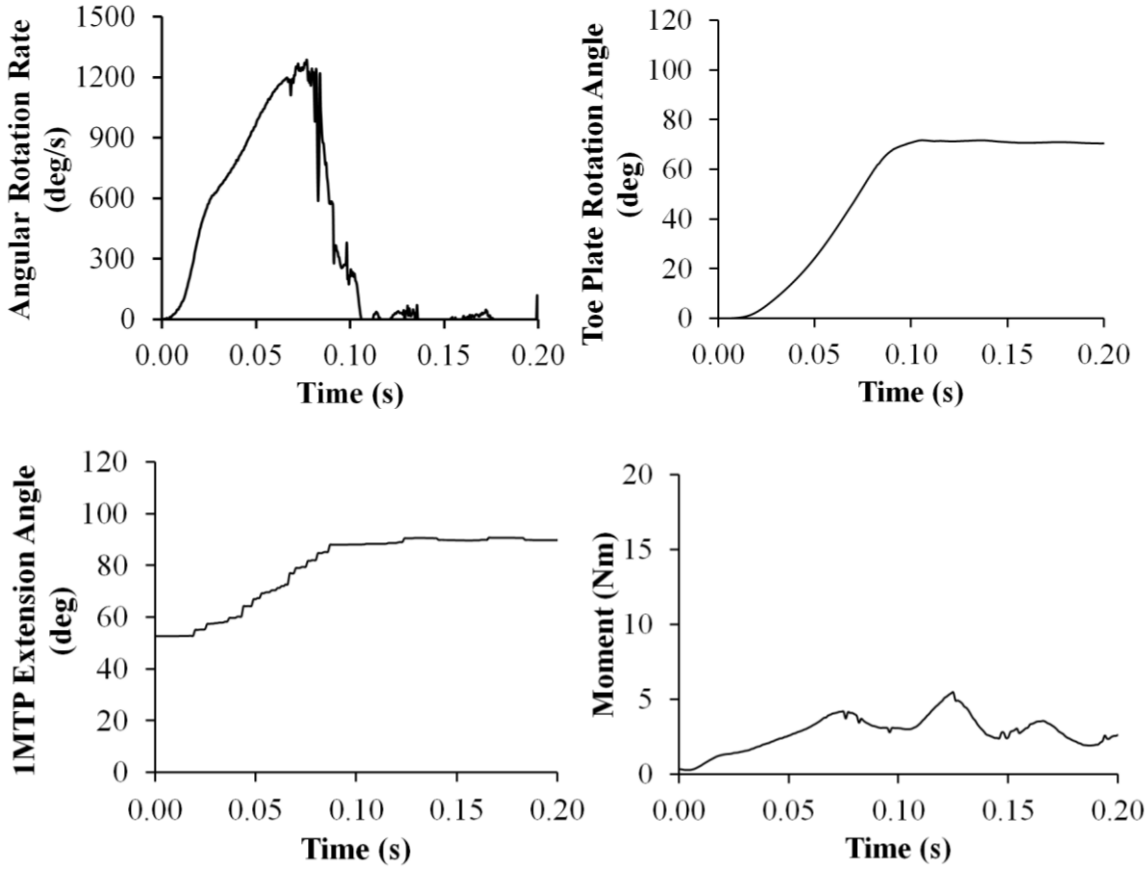

Specimen #411 L

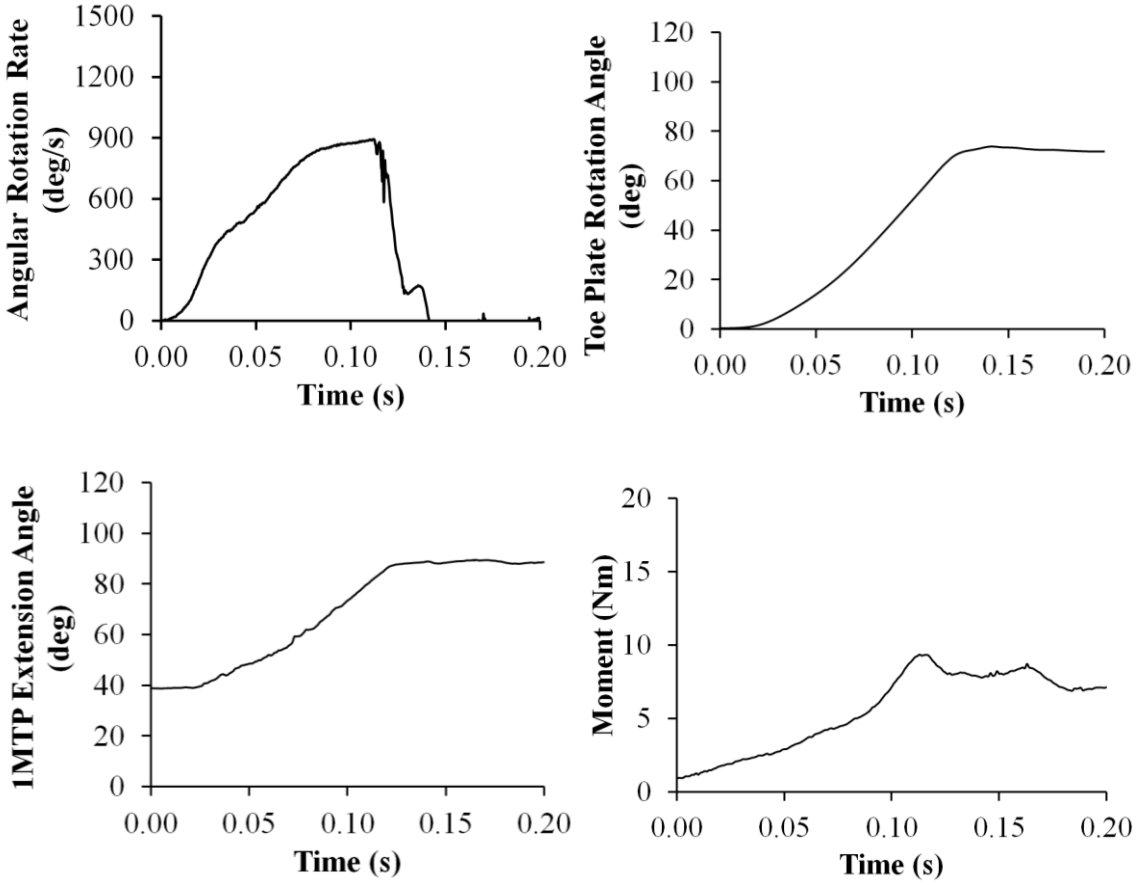

Specimen #416 R

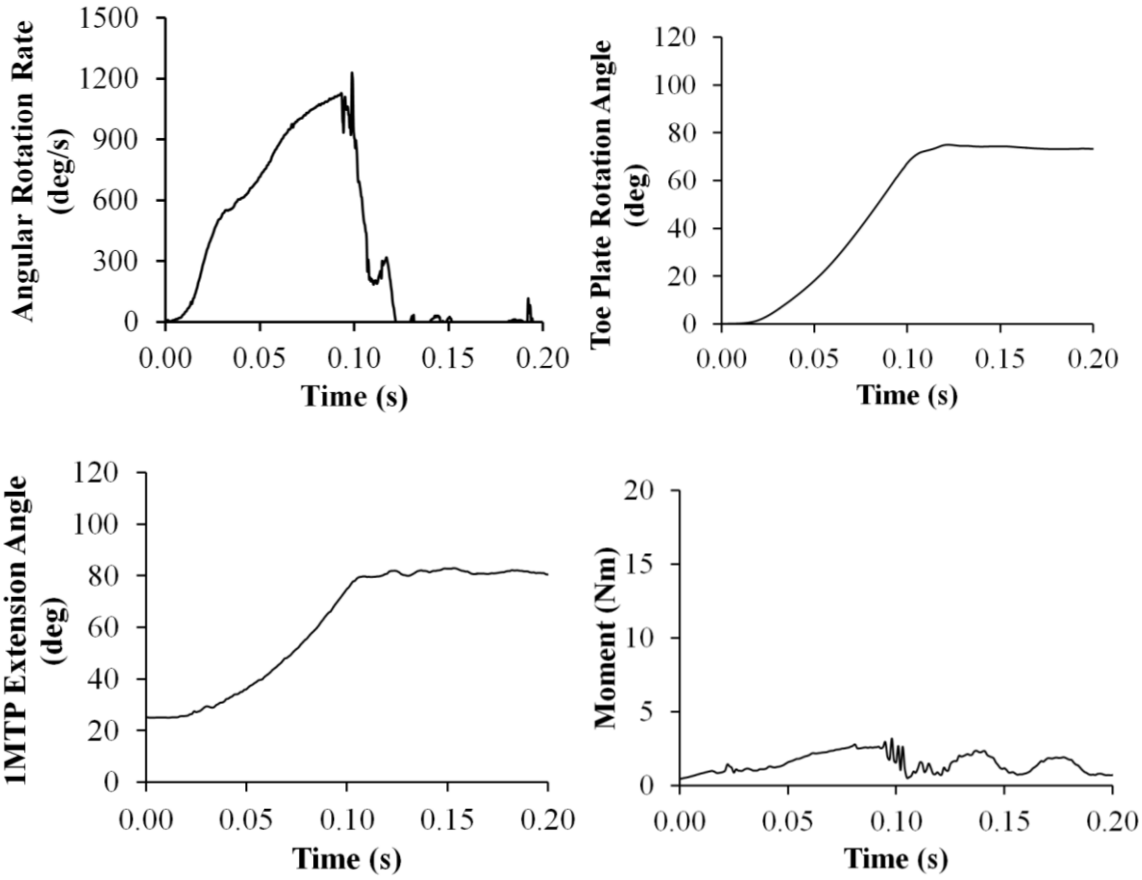

Specimen #486 L

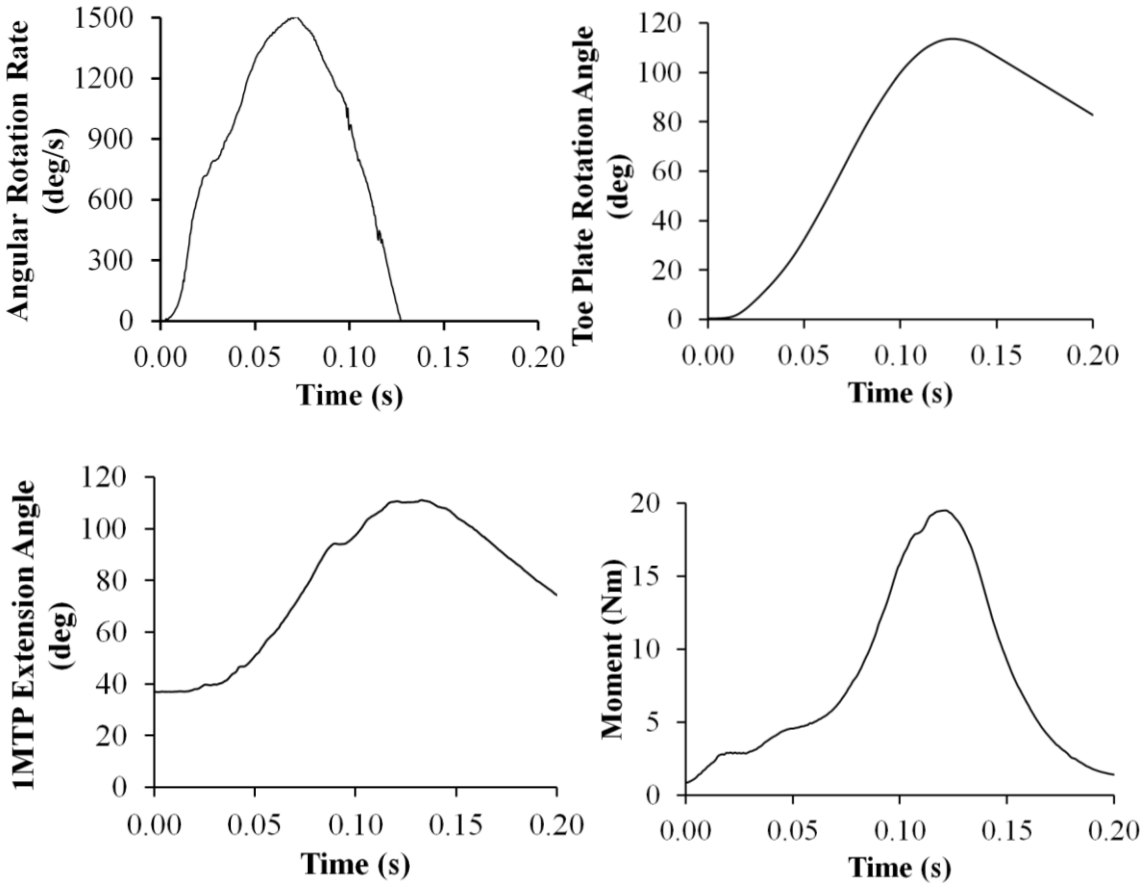

Specimen #486 R

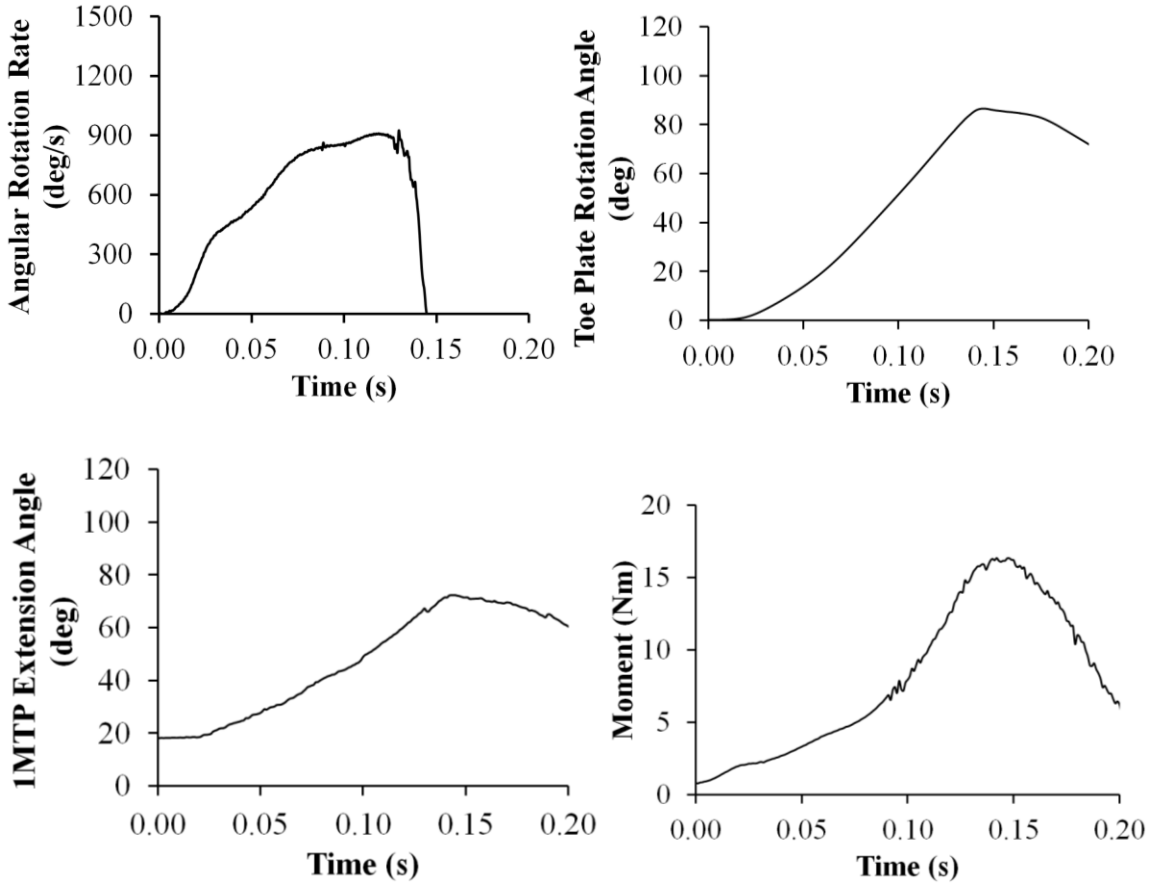

Specimen #487 L

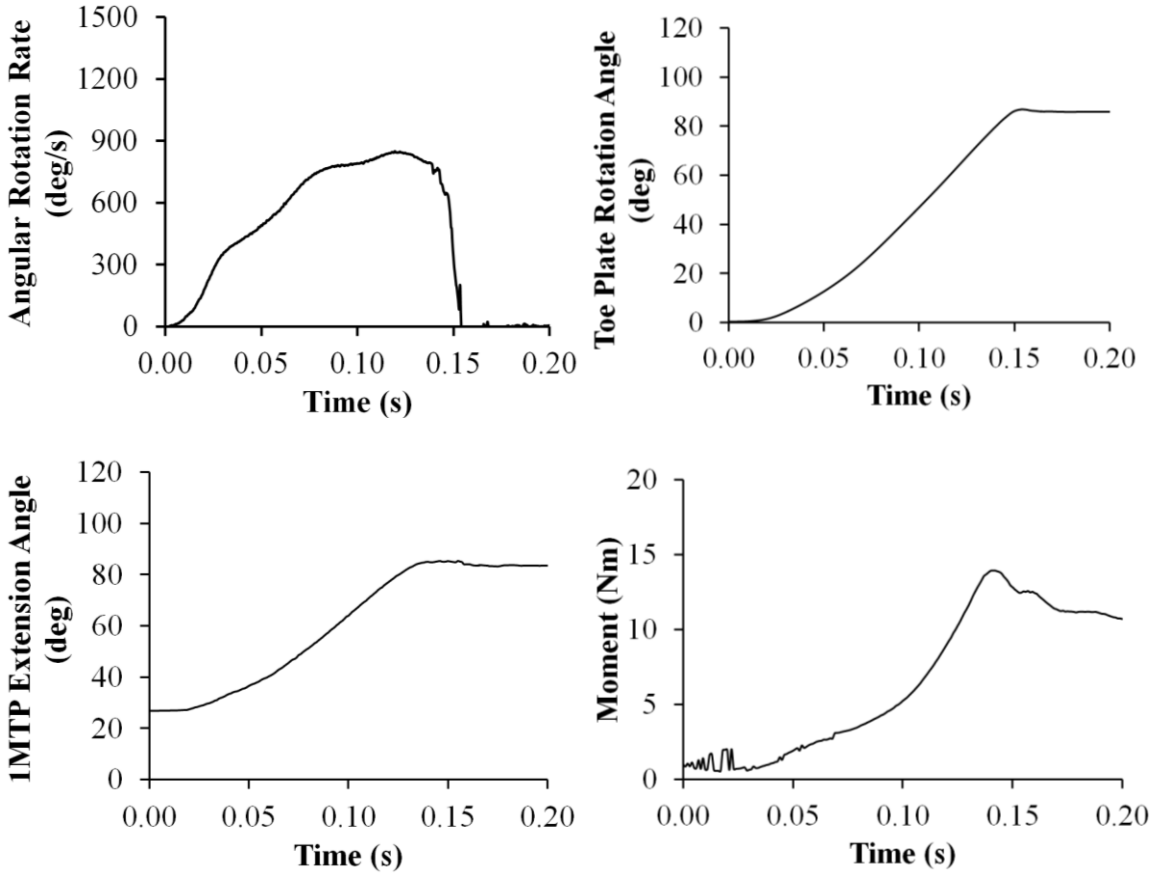

Specimen #487 R

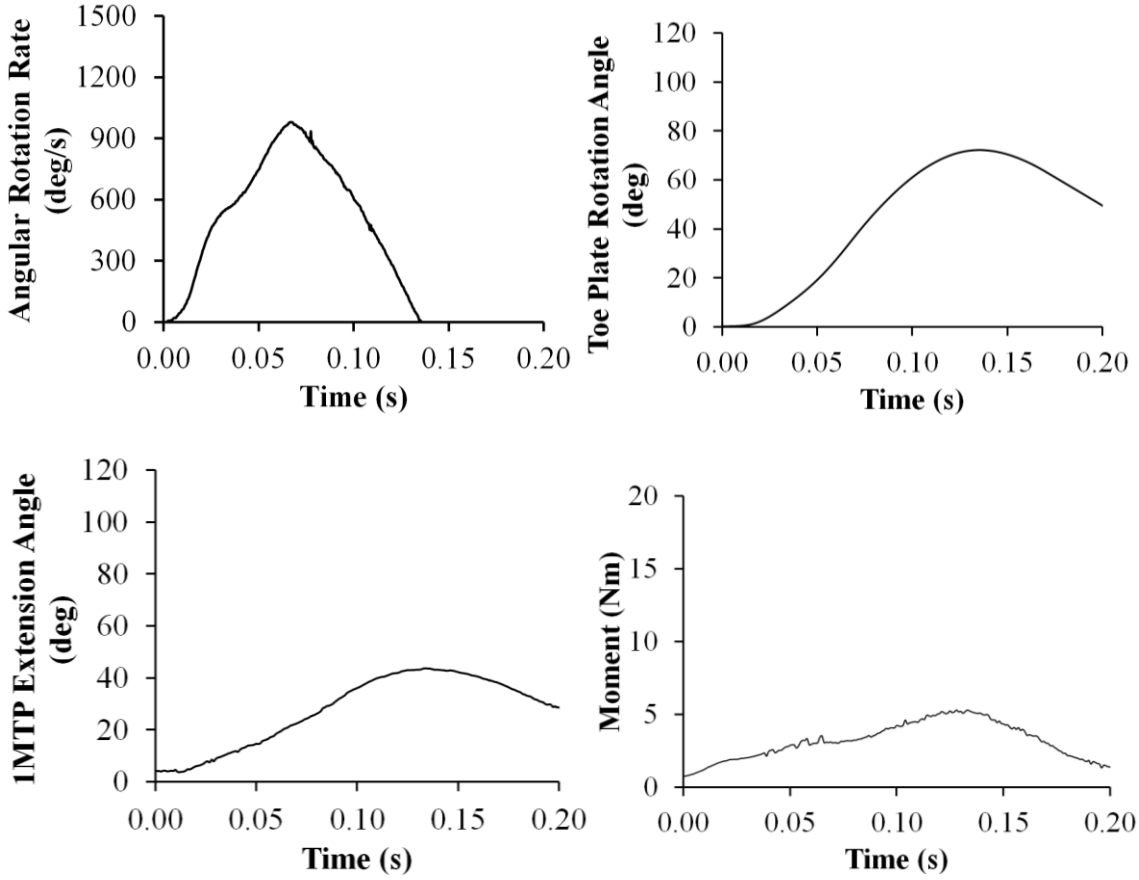

Specimen #488 L

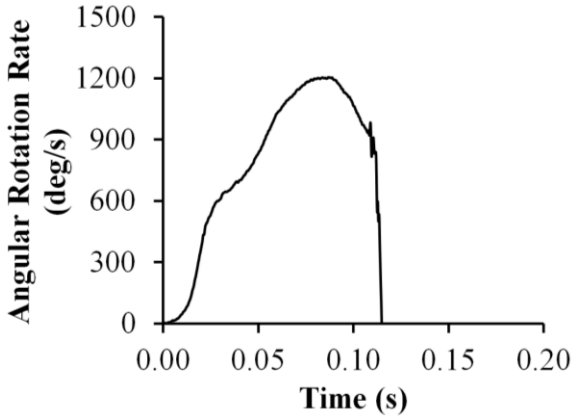

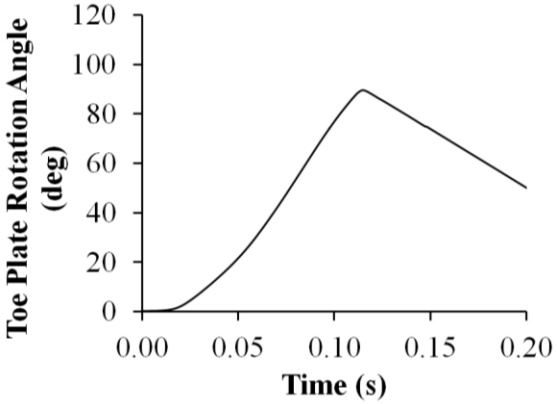

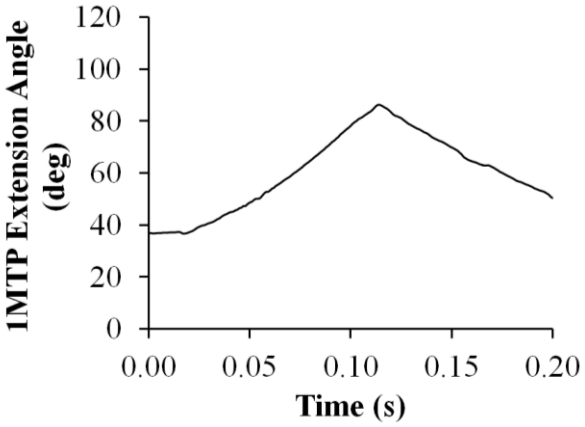

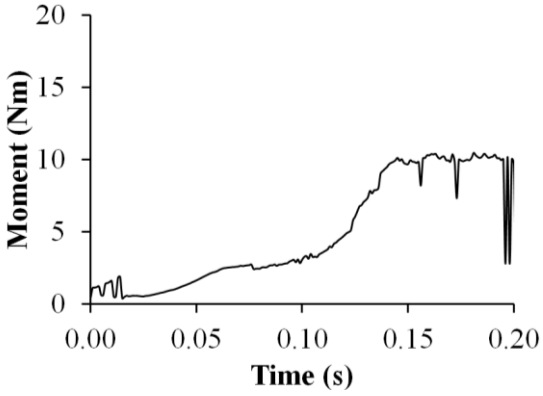

Specimen #490 L

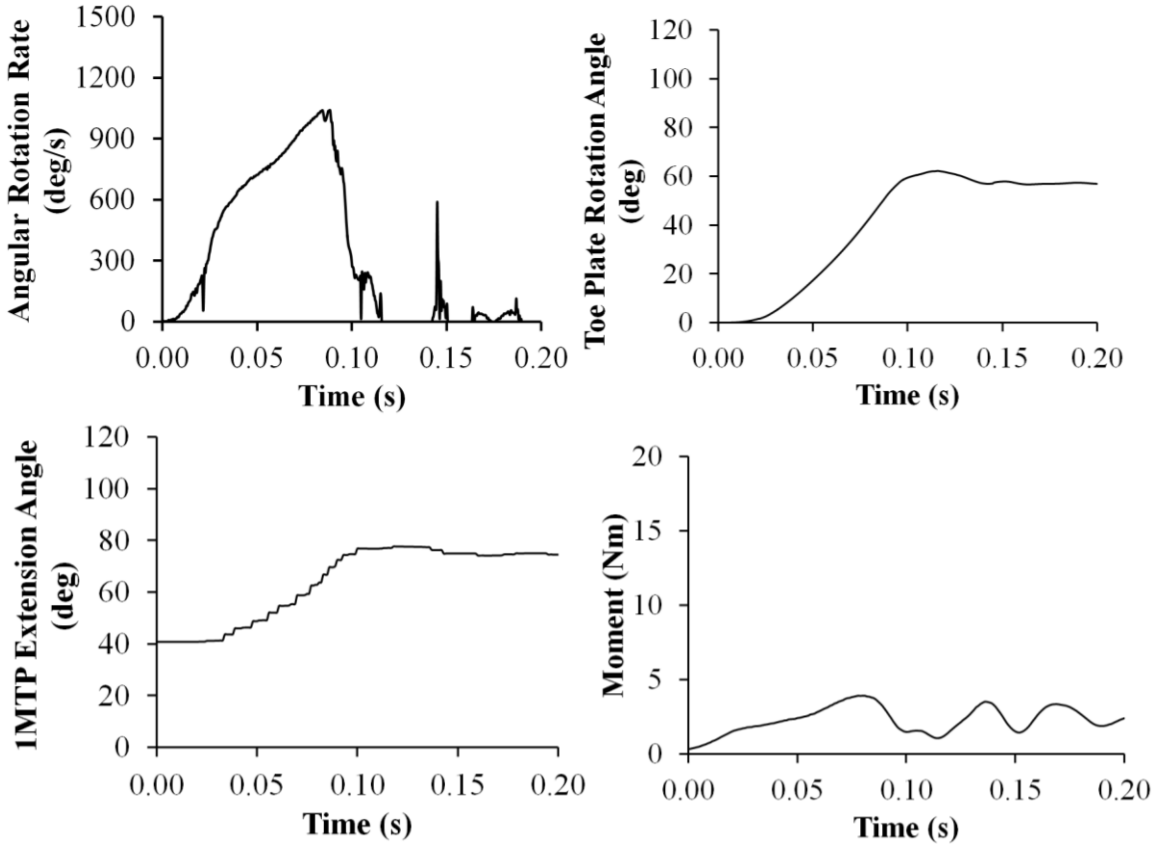

Specimen #490 R

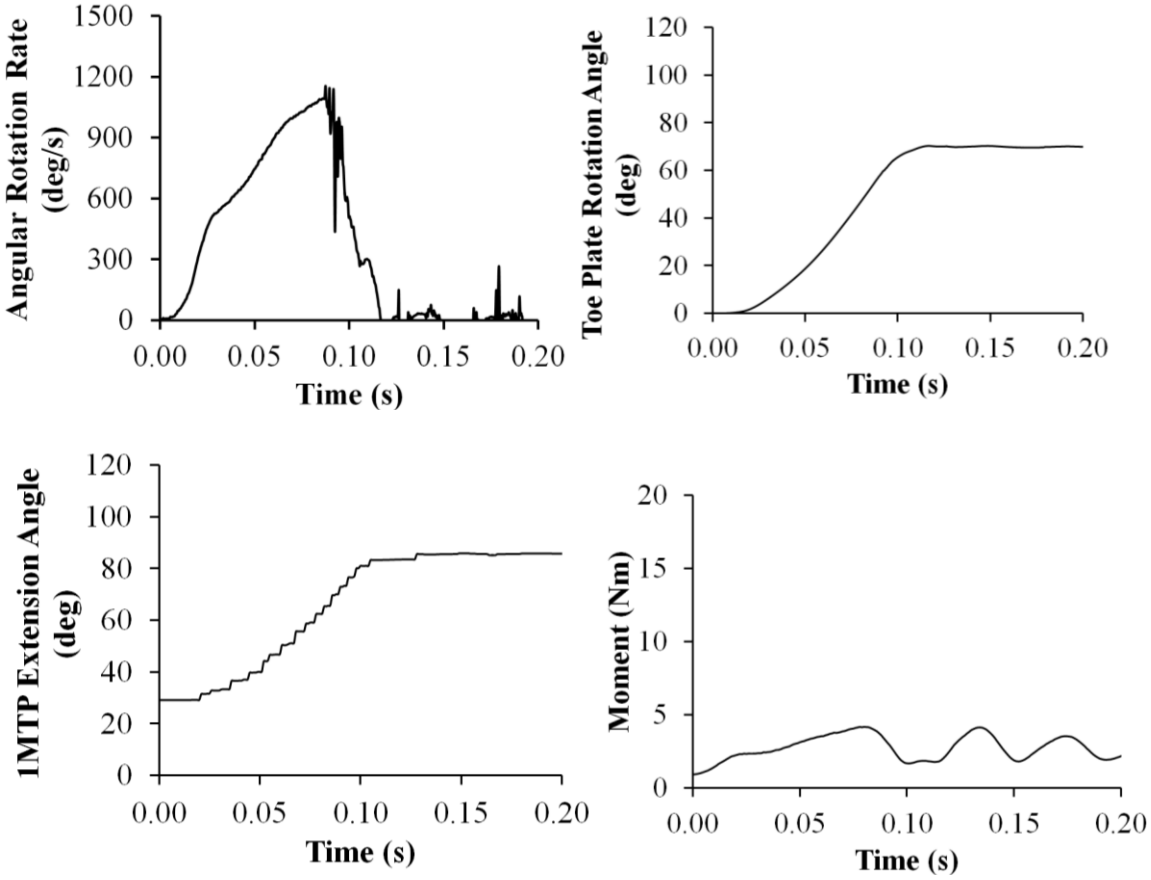

Specimen #492 L

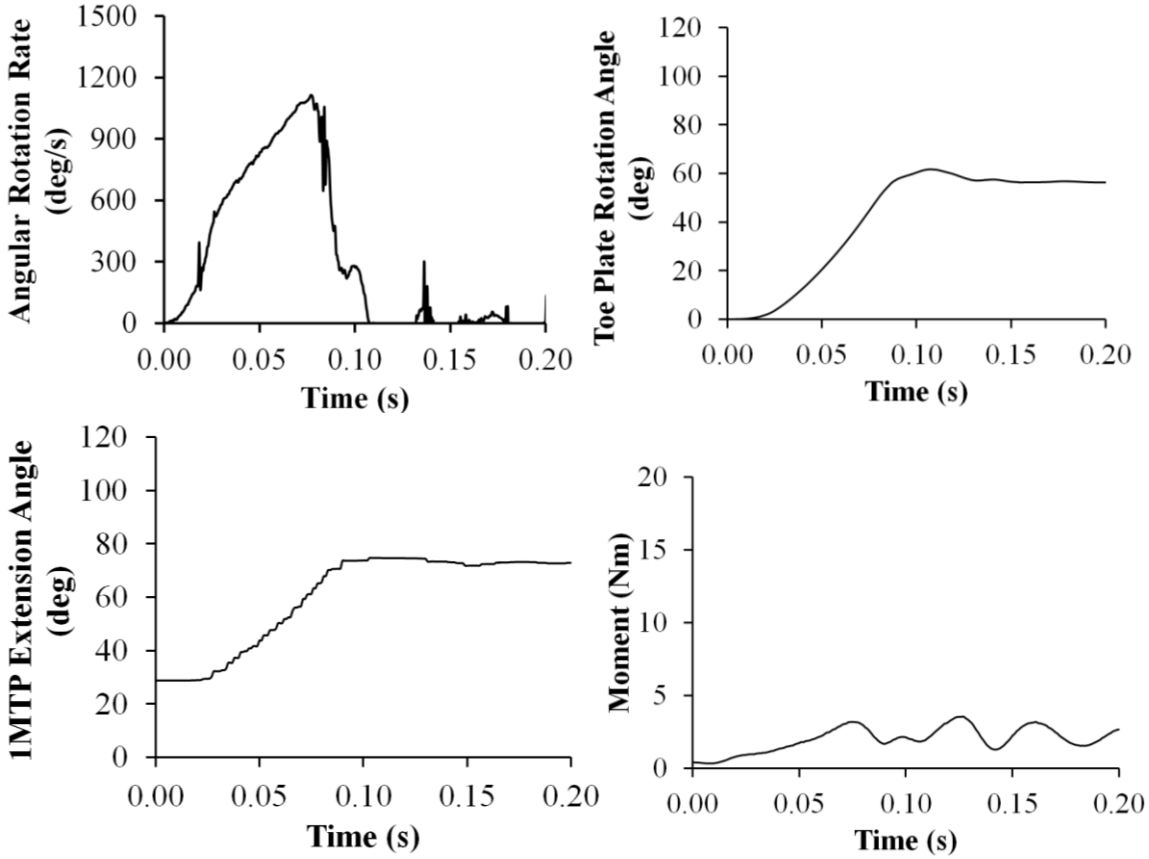

Specimen #492 R

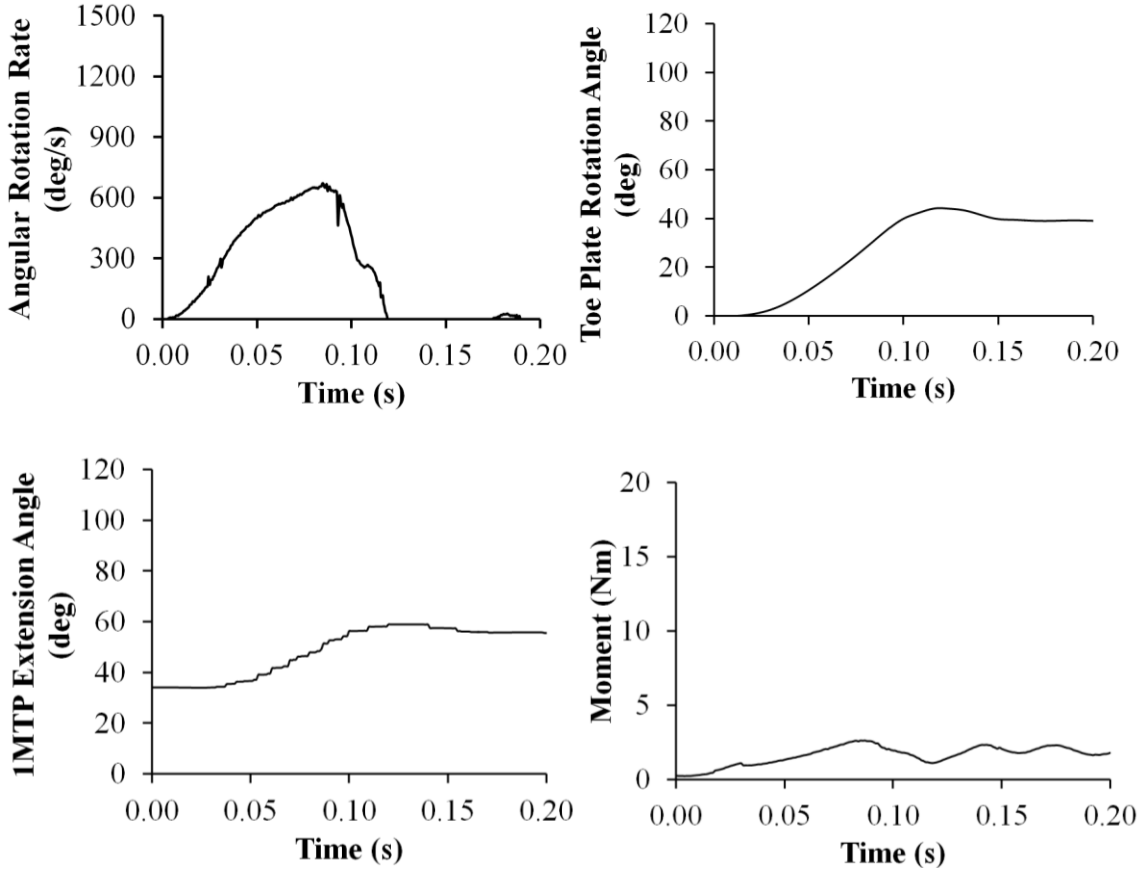

Specimen #495 R

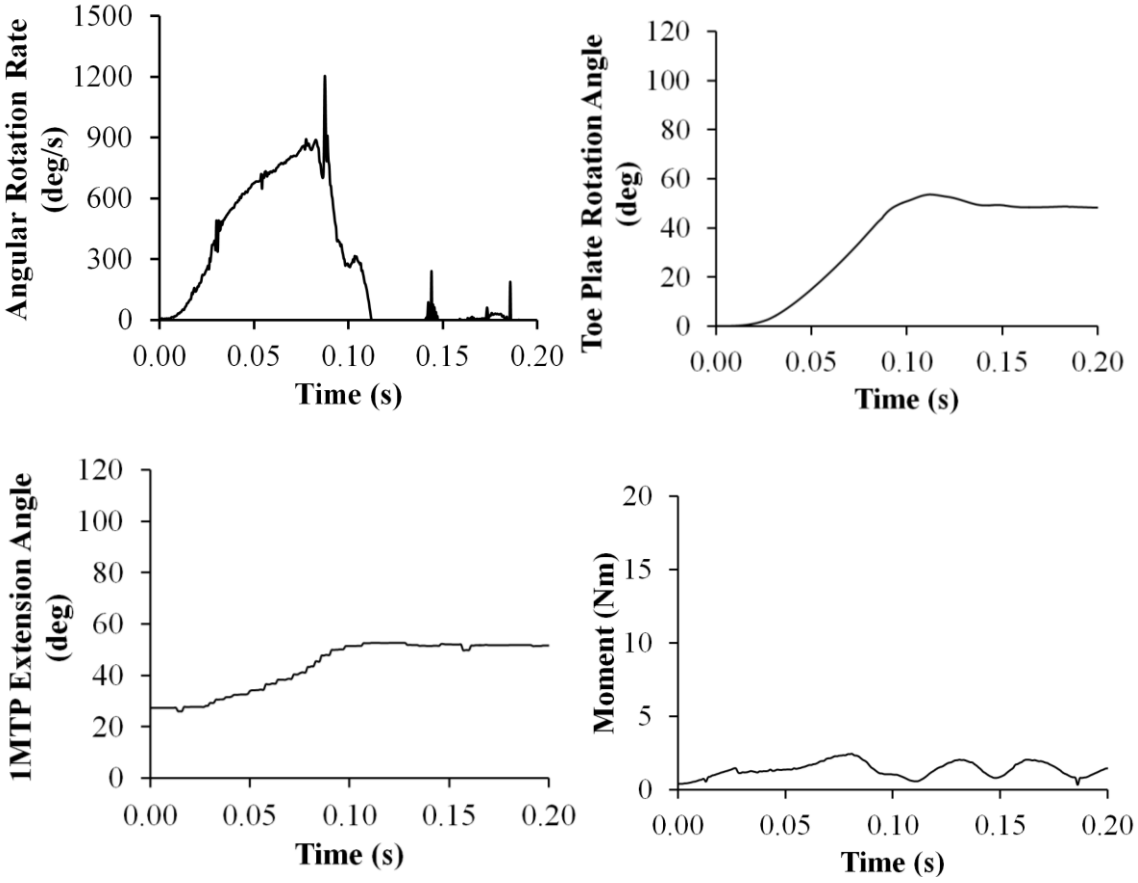

Specimen #496 L

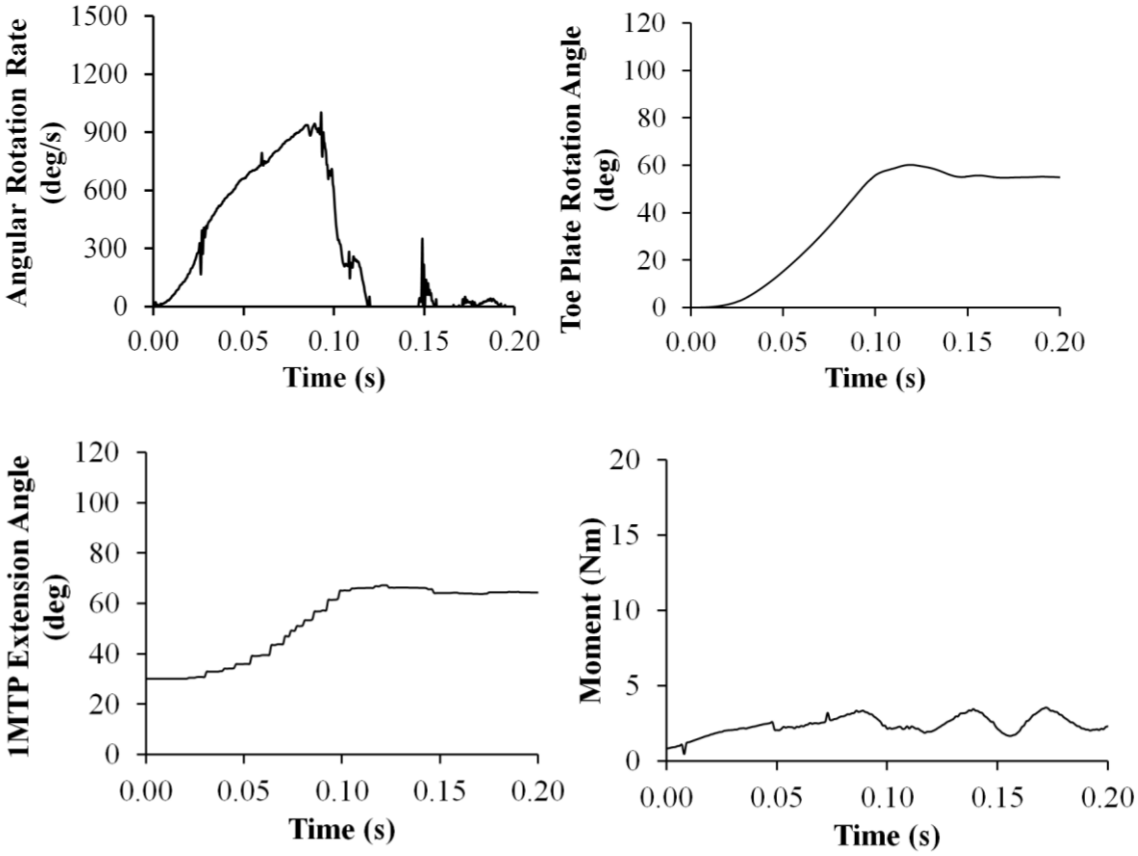

Specimen #496 R